J|A|C|S ARTICLES

Published on Web 07/09/2010

M═N$_\alpha$ Cycloaddition and N$_\alpha$−N$_\beta$ Insertion in the Reactions of Titanium Hydrazido Compounds with Alkynes: A Combined Experimental and Computational Study

A. Daniel Schofield,[†] Ainara Nova,[‡] Jonathan D. Selby,[†] Catherine D. Manley,[†] Andrew D. Schwarz,[†] Eric Clot,*[,‡] and Philip Mountford*[,†]

Chemistry Research Laboratory, Department of Chemistry, University of Oxford, Mansfield Road, Oxford OX1 3TA, U.K., and Institut Charles Gerhardt, Université Montpellier 2, CNRS 5253, cc 1501, Place Eugène Bataillon, 34095 Montpellier Cedex 5, France

Received April 29, 2010; E-mail: eric.clot@univ-montp2.fr; philip.mountford@chem.ox.ac.uk

Abstract: A combined experimental and DFT study of the reactions of diamide-amine supported titanium hydrazides with alkynes is presented. Reaction of Ti(N$_2$N^{py})(NNPh$_2$)(py) (**1**, N$_2$N^{py} = (2-NC$_5$H$_4$)CMe(CH$_2$NSiMe$_3$)$_2$) with terminal and internal aryl alkynes ArCCR (Ar = Ph or substituted phenyl, R = Me or H) at room temperature gave the fully authenticated azatitanacyclobutenes Ti(N$_2$N^{py}){N(NPh$_2$)C(R)CAr} *via* ArCCR [2 + 2] cycloaddition to the Ti═N$_\alpha$ bond of the hydrazide ligand. In contrast, reaction of **1** with PhCCMe at 60 °C, or of Ti(N$_2$N^{Me})(NNPh$_2$)(py) (**11**, N$_2$N^{Me} = MeN(CH$_2$CH$_2$NSiMe$_3$)$_2$) with RCCMe (R = Me, Ph or substituted phenyl) at room temperature or below, gave vinyl imido compounds of the type Ti(N$_2$N$^{R'}$){NC(R)C(Me)NPh$_2$}(py), in which RCCMe had undergone net insertion into the N$_\alpha$−N$_\beta$ bond. These are the first examples of this type of reaction for any metal hydrazide. The reaction of **11** with PhCCMe had the activation parameters $\Delta H^{\ddagger}$ = 18.8(4) kcal mol^{-1}, $\Delta S^{\ddagger}$ = 1(1) cal mol^{-1} K^{-1} and $\Delta G^{\ddagger}_{298}$ = 18.5(7) kcal mol^{-1}. Mechanistic and DFT studies for **1** and **11** found that the N$_\alpha$−N$_\beta$ insertion event is preceded by alkyne cycloaddition to Ti═N$_\alpha$, and that N$_\alpha$−N$_\beta$ bond "insertion" is really an intramolecular N$_\alpha$ atom migration process within the azatitanacyclobutenes following intramolecular chelation of NPh$_2$ of the hydrazide ligand. Electron-withdrawing aryl groups on ArCCMe stabilize the azatitanacyclobutenes and also promote a specific regiochemistry (Ar*C* carbon bound to Ti). This in turn defines the regiochemistry of the overall N$_\alpha$−N$_\beta$ insertion reaction (Ar*C* carbon bound to N$_\alpha$). In contrast, electron-releasing aryl groups promote the final N$_\alpha$ migration stage of the mechanism, and a Hammett analysis of the rates of insertion of (4-C$_6$H$_4$X)CCMe into the N$_\alpha$−N$_\beta$ bond of **11** found a reaction constant, ρ, of −0.74(5), consistent with NPA charge changes of Ar*C* along the DFT reaction coordinate.

Introduction

Terminal transition metal hydrazide(2−) or isodiazene(0) compounds (L)M═NNR$_2$ (R = H, alkyl or aryl) have been of ongoing interest for over 30 years.[1−3] Initial studies focused on molybdenum and tungsten derivatives in the context of the biological conversion of dinitrogen to ammonia.[4−6] Both the stoichiometric Chatt[7−10] and catalytic Schrock[11,12] model systems involve (L)M═NNH$_2$ intermediates immediately prior to the key N$_\alpha$−N$_\beta$ bond-cleavage step, in agreement with computational studies.[13−17] Considerable effort has also been spent on trying to use midtransition metal complexes of the type (L)M═NNR$_2$ as reagents or intermediates for the synthesis of organo−nitrogen products.[4,18,19] However, M═NNR$_2$ functional group reactivity is minimal for these metals, being characterized only by transformations involving the N$_\beta$ atom, namely protonation or reactions involving N$_\beta$−H.[18,20,21] In particular, reactions at the M═N$_\alpha$ bond of the NNR$_2$ group are not seen, and N$_\alpha$−N$_\beta$ bond cleavage only occurs under forcing conditions using external reductants, for example LiAlH$_4$. Structural,[22,23]

[†] University of Oxford.
[‡] Université Montpellier 2.

(1) Johnson, B. F. G.; Haymore, B. L.; Dilworth, J. D. In *Comprehensive Coordination Chemistry*; Wilkinson, G., Gillard, R. D., McCleverty, J. A., Eds.; Pergamon Press: Oxford, 1987; Vol. 2, p 100.
(2) Nugent, W. A.; Mayer, J. M. *Metal-Ligand Multiple Bonds*; Wiley-Interscience: New York, 1988.
(3) Mindiola, D. J. *Angew. Chem., Int. Ed.* **2008**, *47*, 1557.
(4) Fryzuk, M. D. *Chem. Rec.* **2003**, *3*, 2.
(5) MacKay, B. A.; Fryzuk, M. D. *Chem. Rev.* **2004**, *104*, 385.
(6) Kozak, C. M.; Mountford, P. *Angew. Chem., Int. Ed.* **2004**, *43*, 1186.
(7) Chatt, J.; Pearman, A. J.; Richards, R. L. *Nature* **1975**, *253*, 39.
(8) Pickett, C. J.; Leigh, G. J. *J. Chem. Soc., Chem. Commun.* **1981**, 1033.
(9) Hussain, W.; Leigh, G. J.; Pickett, C. J. *J. Chem. Soc., Chem. Commun.* **1982**, 747.
(10) Pickett, C. J.; Talamarin, J. *Nature* **1985**, *317*, 652.
(11) Yandulov, D. V.; Schrock, R. R. *Science* **2003**, 76.
(12) Schrock, R. R. *Acc. Chem. Res.* **2005**, *38*, 955.
(13) Stephan, G. C.; Sivasankar, C.; Studt, F.; Tuczek, F. *Chem.—Eur. J.* **2008**, *14*, 644.
(14) Studt, F.; Tuczek, F. *Angew. Chem., Int. Ed.* **2005**, *44*, 5639.
(15) Schrock, R. R. *Angew. Chem., Int. Ed.* **2008**, *47*, 5512.
(16) Schenk, S.; Kirchner, B.; Reiher, M. *Chem.—Eur. J.* **2009**, *15*, 5073.
(17) Schenk, S.; Le Guennic, B.; Kirchner, B.; Reiher, M. *Inorg. Chem.* **2008**, *47*, 3634.
(18) Hidai, M. *Coord. Chem. Rev.* **1999**, *185−186*, 99.
(19) Ohki, Y.; Fryzuk, M. D. *Angew. Chem., Int. Ed.* **2007**, *46*, 3180.
(20) Fryzuk, M. D.; Johnson, S. A. *Coord. Chem. Rev.* **2000**, *200−202*, 379.
(21) Hidai, M. *Chem. Rev.* **1995**, *95*, 1115.

10.1021/ja1036513

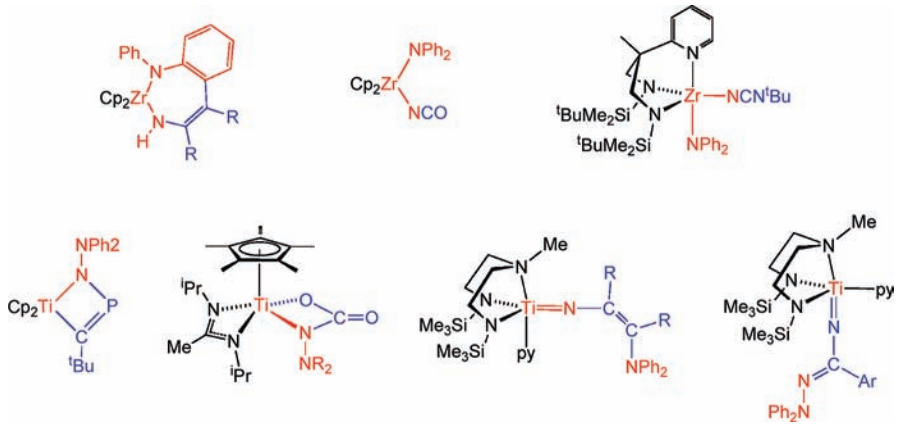

Figure 1. Examples of products formed between terminal Group 4 hydrazides and organic substrates. The atoms of the original M═NNR$_2$ group are shown in red; those of the substrate are in blue.

spectroscopic,[24] and DFT computational[13,14,25,26] data explain this: for mid to later metals "NNR$_2$" is best viewed as a neutral isodiazene :N═NR$_2$ (formally (L)M←:N═NR$_2$). The more dative (donor/acceptor) nature of the M←:N$_\alpha$ bond and multiple bond character of N$_\alpha$═N$_\beta$ reduces the intrinsic reactivity at these two sites.

Although a handful of reports of terminal hydrazides of titanium[27,28] and zirconium[29] appeared some time ago, the first crystallographically characterized titanium example only appeared in 2004.[30] Until this time, Bergman's Cp$_2$Zr(NNPh$_2$)(DMAP)[29] was the sole structurally authenticated example. In contrast to their later metal counterparts, Group 4 M═NNR$_2$ functional groups show very rich and diverse reactivity.[3] Recent DFT calculations[31−34] and a growing pool of structural data[22,23] show that the NNR$_2$ ligands for these metals should be viewed as hydrazide(2−) moieties. The M═N$_\alpha$ bonding (formally a $\sigma^2\pi^4$ triple bond except for metallocene and related "π-loaded" systems) is comparable to that in the corresponding Group 4 imides (L)M═NR (R = alkyl, aryl),[35−37] except that one of the M−N$_\alpha$ π bonds is considerably destabilized by interaction with the N$_\beta$ atom lone pair (in principle making it more reactive). The hydrazide M═N$_\alpha$ bond lengths are comparable to those in Group 4 aryl imides. On the other hand, the N$_\alpha$−N$_\beta$ bond is substantially lengthened compared to Group 6 (L)M═NNR$_2$ complexes as expected from the [N−NR$_2$]$^{2-}$ (hydrazide(2−)) vs N═NR$_2$ (isodiazene) representations, respectively. One therefore expects quite different reactivity patterns between early and later metal hydrazide/isodiazene systems, in much same way that early and later metal alkylidene/carbene systems differ.[2,38]

While synthetic routes to isolable Group 4 hydrazides have steadily become established,[27−34,39−45] their stoichiometric and catalytic reaction chemistry has only been developed during the past few years, and is still very much in its infancy. This is in stark contrast to the position for Group 4 imides, themselves pivotal in the development of metal−heteroatom multiple bonds in general, and which have been extensively studied in terms of reactions, applications, mechanisms and bonding.[46−53] Above all, the combination of an unsaturated, polar M═N$_\alpha$ bond *and* a lengthened and reduced N$_\alpha$−N$_\beta$ bond confers divergent and unique reactivity on the Group 4 M═N−NR$_2$ functional group which undergoes two distinct types of reaction. These apparently involve *either* reaction at the M═N$_\alpha$[28,44,45,54−58] bond (cycloaddition or insertion), *or* cleavage or insertion reactions at the N$_\alpha$−N$_\beta$ bond.[29,41,42,54,55] Figure 1 shows examples of these reaction products. We note that N−N bond cleavage in a hafnium complex has been shown to occur upon addition of CO.[59]

Given the emerging richness and significance of early transition metal hydrazide chemistry, it is now important to understand the relationship between M═N$_\alpha$ cycloaddition and N$_\alpha$−N$_\beta$ cleavage/insertion, and in particular the mechanism(s) of the latter. Although there has been some speculation regarding

(22) Allen, F. H.; Kennard, O. *Chem. Des. Autom. News* **1993**, *8*, 1&31.
(23) Fletcher, D. A.; McMeeking, R. F.; Parkin, D. The United Kingdom Chemical Database Service. *J. Chem. Inf. Comput. Sci.* **1996**, *36*, 746; The UK Chemical Database Service: CSD version 5.31, updated May 2010.
(24) Lehnert, N.; Tuczek, F. *Inorg. Chem.* **1999**, *38*, 1659.
(25) Mersmann, K.; Horn, K. H.; Bores, N.; Lehnert, N.; Studt, F.; Paulat, F.; Peters, G.; Ivanovic-Burmazovic, I.; van Eldik, R.; Tuczek, F. *Inorg. Chem.* **2005**, *44*, 3031.
(26) Lehnert, N.; Tuczek, F. *Inorg. Chem.* **1999**, *38*, 1671.
(27) Wiberg, N.; Haring, H.-W.; Huttner, G.; Friedrich, P. *Chem. Ber.* **1978**, *111*, 2708.
(28) Blake, A. J.; McInnes, J. M.; Mountford, P.; Nikonov, G. I.; Swallow, D.; Watkin, D. J. *J. Chem. Soc., Dalton Trans.* **1999**, 379.
(29) Walsh, P. J.; Carney, M. J.; Bergman, R. G. *J. Am. Chem. Soc.* **1991**, *113*, 6343.
(30) Li, Y.; Shi, Y.; Odom, A. L. *J. Am. Chem. Soc.* **2004**, *126*, 1794.
(31) Parsons, T. B.; Hazari, N.; Cowley, A. R.; Green, J. C.; Mountford, P. *Inorg. Chem.* **2005**, *44*, 8442.
(32) Patel, S.; Li, Y.; Odom, A. L. *Inorg. Chem.* **2007**, *46*, 6373.
(33) Herrmann, H.; Fillol, J. L.; Gehrmann, T.; Enders, M.; Wadepohl, H.; Gade, L. H. *Chem.—Eur. J.* **2008**, *14*, 8131.
(34) Selby, J. D.; Manley, C. D.; Schwarz, A. D.; Clot, E.; Mountford, P. *Organometallics* **2008**, *27*, 6479.
(35) Kaltsoyannis, N.; Mountford, P. *J. Chem. Soc., Dalton Trans.* **1999**, 781.
(36) Cundari, T. R. *Chem. Rev.* **2000**, *100*, 807.
(37) Bolton, P. D.; Clot, E.; Cowley, A. R.; Mountford, P. *J. Am. Chem. Soc.* **2006**, *128*, 15005.
(38) Schrock, R. R. *J. Chem. Soc., Dalton Trans.* **2001**, 2541.
(39) Thorman, J. L.; Woo, L. K. *Inorg. Chem.* **2000**, *39*, 1301.
(40) Banerjee, S.; Odom, A. L. *Organometallics* **2006**, *25*, 3099.
(41) Selby, J. D.; Manley, C. D.; Feliz, M.; Schwarz, A. D.; Clot, E.; Mountford, P. *Chem. Commun.* **2007**, 4937.
(42) Herrmann, H.; Fillol, J. L.; Wadepohl, H.; Gade, L. H. *Angew. Chem., Int. Ed.* **2007**, *46*, 8426.
(43) Herrmann, H.; Wadepohl, H.; Gade, L. H. *Dalton Trans.* **2008**, 2111.
(44) Clulow, A. J.; Selby, J. D.; Cushion, M. G.; Schwarz, A. D.; Mountford, P. *Inorg. Chem.* **2008**, *47*, 12049.
(45) Weitershaus, K.; Wadepohl, H.; Gade, L. H. *Organometallics* **2009**, *28*, 3381.
(46) Wigley, D. E. *Prog. Inorg. Chem.* **1994**, *42*, 239.
(47) Mountford, P. *Chem. Commun.* **1997**, 2127.
(48) Gade, L. H.; Mountford, P. *Coord. Chem. Rev.* **2001**, *216−217*, 65.
(49) Duncan, A. P.; Bergman, R. G. *Chem. Rec.* **2002**, *2*, 431.
(50) Odom, A. L. *Dalton Trans.* **2005**, 225.
(51) Hazari, N.; Mountford, P. *Acc. Chem. Res.* **2005**, *38*, 839.

the mechanism of the $N_\alpha-N_\beta$ bond cleavage/insertion reactions of Group 4 hydrazido[3,42,55] and related[60] compounds, no detailed study has yet emerged. We have used a combination of synthetic, mechanistic and DFT methods to understand the intriguing dichotomy between $M{=}N_\alpha$ and $N_\alpha-N_\beta$ bond reactivity of certain titanium hydrazides with alkynes as representative substrates. The conclusions drawn regarding these specific compounds and substrates can be extrapolated to early transition metal hydrazide reactivity in general.

Synthesis and Mechanistic Studies

The metal-catalyzed reactions of alkynes with hydrazines in general are important and topical from an organic synthesis point of view, as variations of the well-established hydroamination reaction with amines RNH_2 (R = alkyl or aryl).[50,61–63] Bergman,[64] Odom[30,65,66] and others[45,67–69] have found that a range of titanium compounds catalyze the hydrohydrazination of allenes or alkynes with hydrazines (N−H bond addition across C≡C). It is proposed[50] that the key step in these reactions (and in the related iminohydrazination reaction[40,70]) involves [2 + 2] cycloaddition to a transient hydrazido intermediate forming azametallacycles, but as yet nothing is known about their electronic and molecular structures, and they have only been characterized spectroscopically in the last 2 years.[45,54] Since the principal synthetic aspects of this work have been communicated,[41,54] only a brief discussion is given here, focusing in particular on the main features of scope, regiochemistry, and stability.

Alkyne Cycloaddition to Ti=N$_\alpha$. Reaction of $Ti(N_2N^{py})(NNPh_2)(py)$ (**1**) with the internal alkynes ArCCMe (Ar = Ph, 4-$C_6H_4CF_3$ or C_6F_5) in benzene at room temperature for 2−6 h gave the [2 + 2] cycloaddition products $Ti(N_2N^{py})\{N(NPh_2)C(Me)CAr\}$ (Ar = Ph (**2**), 4-$C_6H_4CF_3$ (**3**), or C_6F_5 (**4**)) as dark-red microcrystalline solids (eq 1). The regioisomer shown in eq 1 (i.e., with ArC bound to Ti and MeC bound to N_α) were the only isomers observed.

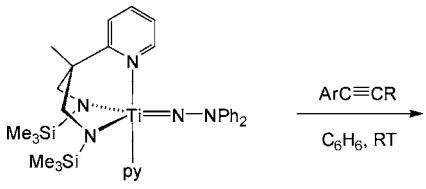

1

ArC≡CR

C_6H_6, RT (1)

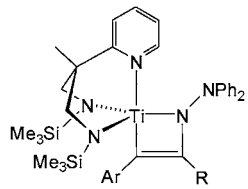

R = Me, Ar = Ph (**2**), 4-$C_6H_4CF_3$ (**3**) or C_6F_5 (**4**)

R = H, Ar = Ph (**5**), Tol (**6**), 3-C_6H_4F (**7**), 4-$C_6H_4CF_3$ (**8**) or C_6F_5 (**9**)

The solid-state structure of **4** (Figure 2) confirms the proposed structures. Compound **1** also reacted cleanly with terminal aryl alkynes ArCCH, forming analogous metallacycles $Ti(N_2N^{py})\{N(NPh_2)C(H)CAr\}$ (Ar = Ph (**5**), Tol (**6**), 3-C_6H_4F (**7**), 4-$C_6H_4CF_3$ (**8**) or C_6F_5 (**9**)). Single crystals of **7** were grown from hexanes. Although these were of rather poor quality, they nonetheless allowed the connectivity to be established (see the Supporting Information), confirming that shown in eq 1. Compounds **2**, **5**, and **6** (containing Ar = Ph or Tol substituents on the metallacyclic ring) were unstable in solution, in the case of **5** and **6** decomposing over ∼10 h at room temperature to unknown mixtures. Furthermore, reaction of **1** with (4-C_6H_4OMe)CCMe formed a complex mixture of products, and with MeCCMe no reaction occurred. In contrast, the other compounds $Ti(N_2N^{py})\{N(NPh_2)C(R)CAr\}$ (Ar = 4-$C_6H_4CF_3$, 3-C_6H_4F or C_6F_5; R = H or Me) with electron-withdrawing aryl groups were stable for at least one week. When followed by ^1H NMR in C_6D_6, the reaction between **1** and PhCCMe formed a ∼55:45 equilibrium mixture of starting hydrazide **1** and product $Ti(N_2N^{py})\{N(NPh_2)C(Ph)CMe\}$ (**2**). In contrast, reaction of **1** in C_6D_6 with ArCCMe (Ar = 4-$C_6H_4CF_3$ or C_6F_5) or any of the

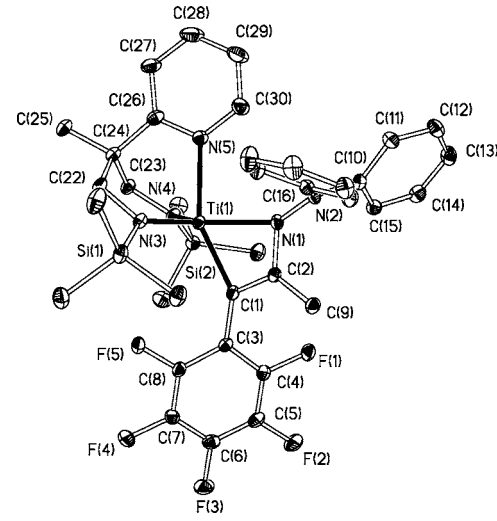

Figure 2. Displacement ellipsoid plot (25% probability) of $Ti(N_2N^{py})\{N(NPh_2)C(Me)C(C_6F_5)\}$ (**4**). H atoms omitted for clarity. Selected distances (Å): Ti(1)−N(1) 2.119(2), Ti(1)−N(3) 1.895(2), Ti(1)−N(4) 1.902(2), Ti(1)−N(5) 2.232(2), Ti(1)−C(1) 2.065(2), N(1)−N(2) 1.418(2), N(1)−C(2) 1.382(3), N(2)−C(10) 1.398(2), N(2)−C(16) 1.416(2), C(1)−C(2) 1.378(3), C(1)−C(3) 1.448(3).

(52) Bolton, P. D.; Mountford, P. *Adv. Synth. Catal.* **2005**, *347*, 355.
(53) Fout, A. R.; Kilgore, U. J.; Mindiola, D. J. *Chem.—Eur. J.* **2007**, *13*, 9428.
(54) Selby, J. D.; Schulten, C.; Schwarz, A. D.; Stasch, A.; Clot, E.; Jones, C.; Mountford, P. *Chem. Commun.* **2008**, 5101.
(55) Gehrmann, T.; Fillol, J. L.; Wadepohl, H.; Gade, L. H. *Angew. Chem., Int. Ed.* **2009**, *48*, 2152.
(56) Weitershaus, K.; Fillol, J. L.; Wadepohl, H.; Gade, L. H. *Organometallics* **2009**, *28*, 4747.
(57) Gehrmann, T.; Fillol, J. L.; Wadepohl, H.; Gade, L. H. *Organometallics* **2010**, *29*, 28.
(58) Tiong, P.-J.; Schofield, A. D.; Selby, J. D.; Nova, A.; Clot, E.; Mountford, P. *Chem. Commun.* **2010**, *46*, 85.
(59) Knobloch, D. J.; Lobkovsky, E.; Chirik, P. J. *Nat. Chem.* **2010**, 2.
(60) Kaplan, A. W.; Polse, J. L.; Ball, G. E.; Andersen, R. A.; Bergman, R. G. *J. Am. Chem. Soc.* **1998**, *120*, 11649.
(61) Bytschkov, I.; Doye, S. *Eur. J. Org. Chem.* **2003**, 935.
(62) Doye, S. *Synlett* **2004**, 1653.
(63) Hultzsch, K. C. *Adv. Synth. Catal.* **2005**, *347*, 367.
(64) Johnson, J. S.; Bergman, R. G. *J. Am. Chem. Soc.* **2001**, *123*, 2923.
(65) Cao, C.; Shi, Y.; Odom, A. L. *Org. Lett.* **2002**, *4*, 2853.
(66) Banerjee, S.; Barnea, E.; Odom, A. L. *Organometallics* **2008**, *27*, 1005.
(67) Ackermann, L.; Born, R. *Tetrahedron Lett.* **2004**, *45*, 9541.
(68) Khedkar, V.; Tillack, A.; Michalik, M.; Beller, M. *Tetrahedron Lett.* **2004**, *45*, 3123.
(69) Tillack, A.; Jiao, H.; Garcia Castro, I.; Hartung, C. G.; Beller, M. *Chem.—Eur. J.* **2004**, *10*, 2410.
(70) Banerjee, S.; Shi, Y.; Cao, C.; Odom, A. L. *J. Organomet. Chem.* **2005**, *690*, 5066.

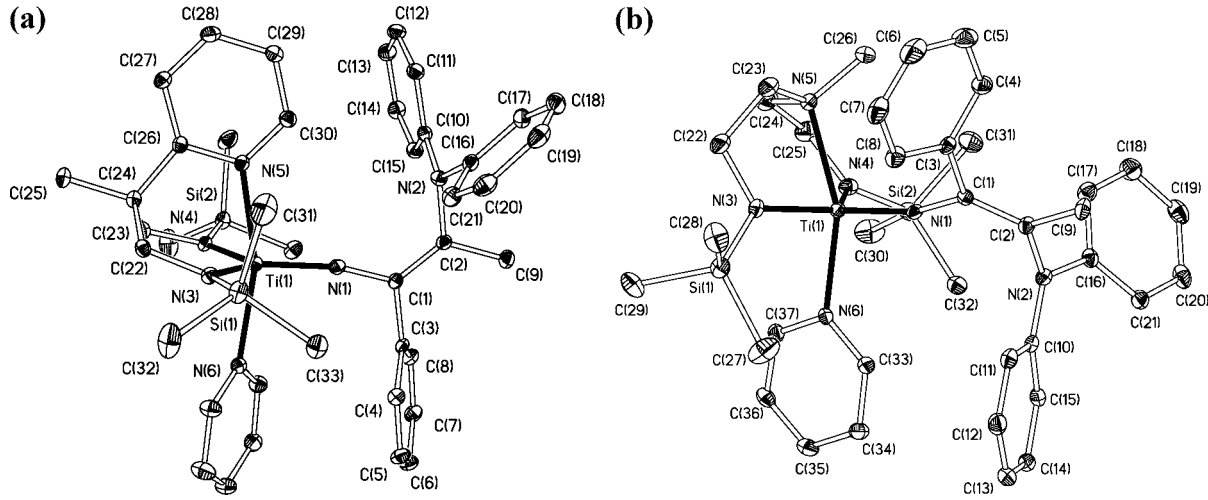

Figure 3. Displacement ellipsoid plots (20% probability) of (a) Ti(N_2N^{py}){NC(Ph)C(Me)NPh_2}(py) (**10**) and (b) Ti(N_2N^{Me}){NC(Ph)C(Me)NPh_2}(py) (**13**). H atoms omitted for clarity. Distances and angles are given in the Supporting Information (SI).

terminal alkynes in eq 1 gave quantitative formation of the corresponding metallacycles and free pyridine. Taken together, these results show that electron-releasing substituents on the alkynes ArCCR destabilize the azatitanacyclobutene products, whereas electron-deficient Ar groups or terminal alkynes tend to give more stable species.

Although [2 + 2] cycloaddition reactions of Group 4 imido compounds with terminal and internal alkynes forming metallacycles are well-established,[46–51,71–77] and hydrazide-derived metallacycles of the type **2**−**9** have been implicated as intermediates in the catalytic hydrohydrazination of alkynes[50] (and in one instance spectroscopically observed[45]), none other than those described herein have yet been isolated or structurally authenticated for any transition metal.

Alkyne Insertion into N_α−N_β. When the equilibrium mixture formed from **1** and PhCCMe in C_6D_6 was allowed to stand for three days at room temperature the new complex Ti(N_2N^{py}){NC(Ph)C(Me)NPh_2}(py) (**10**) was formed as the sole product (eq 2). Heating a mixture of **1** and PhCCMe at 60 °C accelerated the reaction forming **10** within 3 h. Compound **10** is a vinyl imido species formally formed by insertion of PhCCMe into the N_α−N_β bond of **1**. The solid state structure has been determined (Figure 3) and is discussed below. On scale up in toluene, **10** was obtained in 71% isolated yield. Unfortunately, attempts to extend this unique reaction to other alkynes using **1** were unsuccessful. Heating solutions of **1** and ArCCMe (Ar = 4-$C_6H_4CF_3$ or C_6F_5) in C_6D_6 gave only the metallacyclic products **3** and **4**, whereas with ArCCH (Ar = Ph, Tol, 4-$C_6H_4CF_3$ or C_6F_5) mixtures of products were formed.

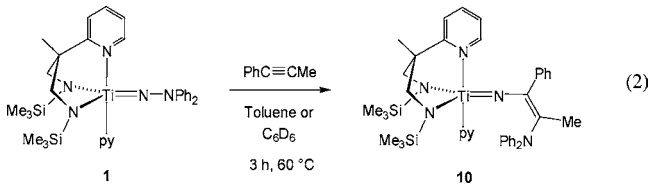

(2)

Encouraged by the formation of the Ti=N_α cycloaddition products **2**−**9** and the N_α−N_β bond insertion reaction giving **10**, we screened a number of other diamide-amine supported titanium hydrazides[34] for their reactions with terminal and internal alkynes. Gratifyingly, Ti(N_2N^{Me})($NNPh_2$)(py) (**11**) readily formed a range of well-defined N_α−N_β insertion products Ti(N_2N^{Me}){NC(R)C(Me)NPh_2}(py) (**12**−**18**, R = Me, Ph or substituted phenyl, eq 3). All of the reactions proceeded readily at room temperature and were quantitative when followed by ^{1}H NMR in C_6D_6. In general, the more electron-rich alkynes ArCCMe (Ar = 4-$C_6H_4{}^t$Bu or 4-C_6H_4OMe) gave the fastest insertion reactions. In contrast to the corresponding reactions of **1** (eq 1), no cycloaddition products were observed at room temperature. A detailed experimental and DFT mechanistic study is presented later on.

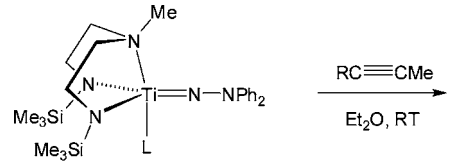

(3)

L = py (**11**) or DMAP (**21**)

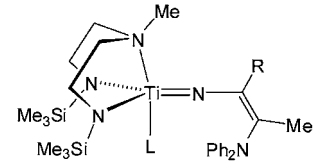

L = py, R = Me (**12**), Ph (**13**), Tol (**14**), 4-$C_6H_4{}^t$Bu (**15**), 4-C_6H_4OMe (**16**), 4-$C_6H_4CF_3$ (**17**) or C_6F_5 (**18**). L = DMAP, R = Ph (**22**)

Extending the reactions of **11** to the dialkyne MeCC(2,3,5,6-C_6F_4)CCMe (**19**) in a 2:1 (**11**:**19**) ratio gave the dinuclear N_α−N_β insertion product **20** (eq 4) in 36% isolated yield.

(71) Polse, J. L.; Andersen, R. A.; Bergman, R. G. *J. Am. Chem. Soc.* **1998**, *120*, 13405.
(72) Ward, B. D.; Maisse-Francois, A.; Mountford, P.; Gade, L. H. *Chem. Commun.* **2004**, 704.
(73) Wang, H.; Chan, H.; Xie, Z. *Organometallics* **2005**, *24*, 3772.
(74) Bolton, P. D.; Feliz, M.; Cowley, A. H.; Clot, E.; Mountford, P. *Organometallics* **2008**, *27*, 6096.
(75) Vujkovic, N.; Ward, B. D.; Maisse-Francois, A.; Wadepohl, H.; Mountford, P.; Gade, L. H. *Organometallics* **2007**, *26*, 5522.
(76) Walsh, P. J.; Baranger, A. M.; Bergman, R. G. *J. Am. Chem. Soc.* **1992**, *114*, 1708.
(77) Basuli, F.; Aneetha, H.; Huffman, J. C.; Mindiola, D. J. *J. Am. Chem. Soc.* **2005**, *127*, 17992.

Reaction of **11** with **19** in a 1:1 ratio gave a mixture of species containing **11** and **20**. However, unidentified mixtures were formed between **11** and terminal alkynes RCCH (R = Ph, $SiMe_3$, 4-$C_6H_4CF_3$), EtCCEt or PhCCPh. No reaction occurred with $Me_3SiCCMe$ either at room temperature or upon heating.

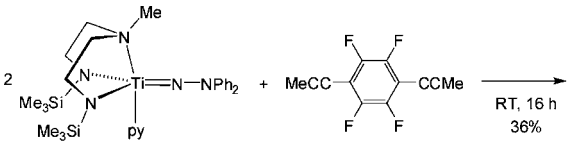

11 **19**

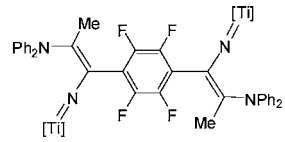

20

[Ti] = $Ti(N_2N^{Me})(py)$

The solid state structures of $Ti(N_2N^{py})\{NC(Ph)C(Me)NPh_2\}(py)$ (**10**) and $Ti(N_2N^{Me})\{NC(Ph)C(Me)NPh_2\}(py)$ (**13**) are shown in Figure 3, and that of $[Ti(N_2N^{Me})\{NCC(Me)NPh_2\}(py)]_2(\mu-2,3,5,6\text{-}C_6F_4)$ (**20**) is given in the SI. Single crystals of **18** were also analyzed but found to be poor diffractors. Nonetheless, its connectivity could be confidently established (see the SI) which was analogous to that for **10** and **13**.

All three compounds **10**, **13** and **20** possess trigonal bipyramidal Ti atoms with the N_{amide} atoms and N_α of the new vinyl imido ligand occupying the equatorial coordination sites. The $Ti{=}N_\alpha$ bond distances (avg. 1.760 Å) are equivalent within error and consistent with a formal triple bond as previously established for compounds of the general type $Ti(N_2N^R)(NR')(py)$ (R′ = alkyl, aryl, NPh_2; R = Me, $SiMe_3$ and py).[34,75,78,79] Overall, the new vinyl imides **10**, **13** and **20** have very similar structures, and the key distances and angles around titanium are comparable to the starting hydrazides themselves.

Titanium vinyl imido compounds have previously been prepared by reaction of sources of alkylidene compounds such as $Cp_2Ti{=}CH_2$ with organic nitriles.[80,81] These vinyl imides can have a rich reaction chemistry with other unsaturated substrates *via* [4 + 2] cycloaddition reactions. Although cleavage reactions of the $N_\alpha{-}N_\beta$ bond of terminal Group 4 hydrazide and related ligands with a number of unsaturated substrates (including alkynes) have been previously reported (see Introduction), the reactions in eqs 2, 3, and 4 are unique examples of net substrate insertion into the $N_\alpha{-}N_\beta$ bond of a terminal hydrazide ligand.

Mechanistic Investigations of the $N_\alpha{-}N_\beta$ Insertion Reaction. The reaction between $Ti(N_2N^{Me})(NNPh_2)(py)$ (**11**) and PhCCMe in toluene-d_8 was monitored by ^{1}H NMR spectroscopy between −50 and 0 °C in the presence of 1,4-dimethoxybenzene as an internal standard. Between −50 and −40 °C there was no reaction between **11** and the alkyne. Above −40 to −35 °C, the starting materials were quantitatively converted to the $N_\alpha{-}N_\beta$ insertion product $Ti(N_2N^{Me})\{NC(Ph)C(Me)NPh_2\}(py)$ (**13**). No intermediates or other product regioisomers were observed, and the reaction was complete within two hours at 0 °C. The corresponding reaction of $Ti(N_2N^{py})(NNPh_2)(py)$ (**1**) and PhCCMe was also followed by ^{1}H NMR. The first-formed equilibrium mixture of **1**, PhCCMe, metallacycle $Ti(N_2N^{py})\{N(NPh_2)C(Me)CPh\}$ (**2**) and pyridine was quantitatively converted to $Ti(N_2N^{py})\{NC(Ph)C(Me)NPh_2\}(py)$ (**10**) at room temperature over three days (or at 60 °C over 3 h). Again no other regioisomer of **10** was observed. Since the reaction between **11** and PhCCMe is significantly faster than for **1**, and tolerates a wider range of substrates RCCR′ (*cf.* eq 3), it was the one selected for detailed further study.

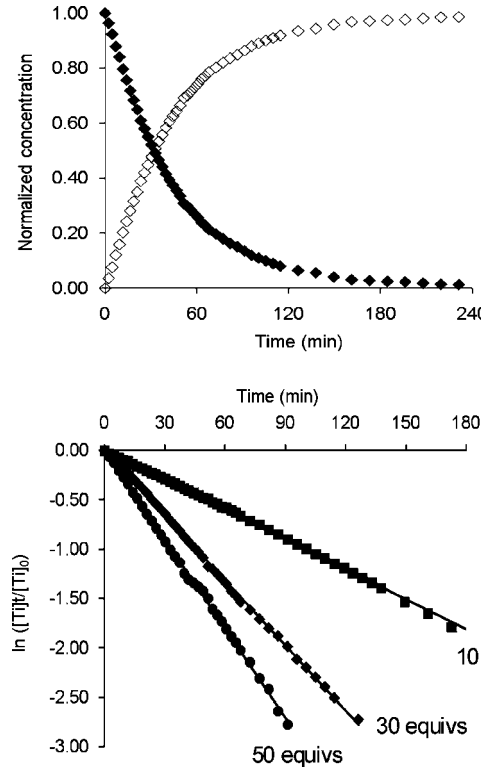

Figure 4. (Top) Decay of $Ti(N_2N^{Me})(NNPh_2)(py)$ (**11**, filled diamonds) and growth of $Ti(N_2N^{Me})\{NC(Ph)C(Me)NPh_2\}$ (**13**, hollow diamonds) with time for the reaction between **11** and PhCCMe (30 equiv) at −26 °C. (Bottom) Pseudo-first-order log plots for the reaction of $Ti(N_2N^{Me})(NNPh_2)(py)$ (**11**) with PhCCMe (10, 30, 50 equiv) at −26 °C. The best-fit lines show $r^2 = 0.999$ in all cases.

When the reaction between **11** and an excess of PhCCMe (10−50 equiv) was followed at −26 °C in toluene-d_8 the decay of hydrazide starting material (and evolution of **13**) followed well-behaved pseudo-first-order kinetics with respect to Ti as illustrated in Figure 4. However, as shown in Figure 5 (top), the observed rate constants (k_{obs}) obtained from the linear log plots do not scale linearly with the equivalents of PhCCMe used. At high values of [PhCCMe]:[**11**] the onset of saturation kinetics is very evident. In contrast, the corresponding double-reciprocal plot (Figure 5, bottom) is linear over the range of PhCCMe equivalents used. At first sight, the data in Figures 4 and 5 are consistent with the general process outlined in Scheme 1 in which dissociation of py from **11** forms a reactive pyridine-free intermediate **11′** prior to the rate-limiting step (or steps), the rate constant for which is denoted as "k_2". Scheme 1 is

(78) Pugh, S. M.; Clark, H. S. C.; Love, J. B.; Blake, A. J.; Cloke, F. G. N.; Mountford, P. *Inorg. Chem.* **2000**, *39*, 2001.
(79) Blake, A. J.; Collier, P. E.; Gade, L. H.; Mountford, P.; Lloyd, J.; Pugh, S. M.; Schubart, M.; Skinner, M. E. G.; Trösch, J. M. *Inorg. Chem.* **2001**, *40*, 870.
(80) Doxsee, K. M.; Farahi, J. B.; Hope, H. *J. Am. Chem. Soc.* **1991**, *113*, 8889.
(81) Bailey, B. C.; Fout, A. R.; Fan, H.; Tomaszewski, J.; Huffman, J. C.; Gary, J. B.; Johnson, M. J. A.; Mindiola, D. J. *J. Am. Chem. Soc.* **2007**, *129*, 2234.

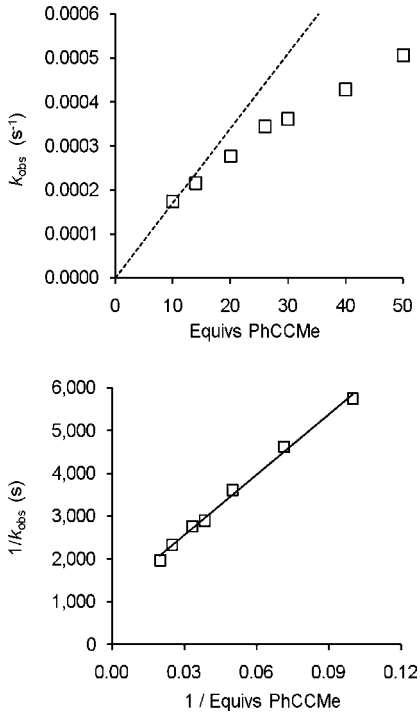

Figure 5. Top: plot of k_{obs} vs equivalents of alkyne for the reaction of $Ti(N_2N^{Me})(NNPh_2)(py)$ (**11**) with PhCCMe; the dotted line is that expected for a linear relationship between k_{obs} and equivalents based on extrapolation from the first data point (10 equiv). Bottom: the corresponding double-reciprocal plot. The linear fit ($r^2 = 0.995$) gives an intercept of $1/k_{obs} = 1.15(8) \times 10^3$ s.

Scheme 1. Experimentally Implicated Steps in the Formation of **13** from **11** and PhCCMe

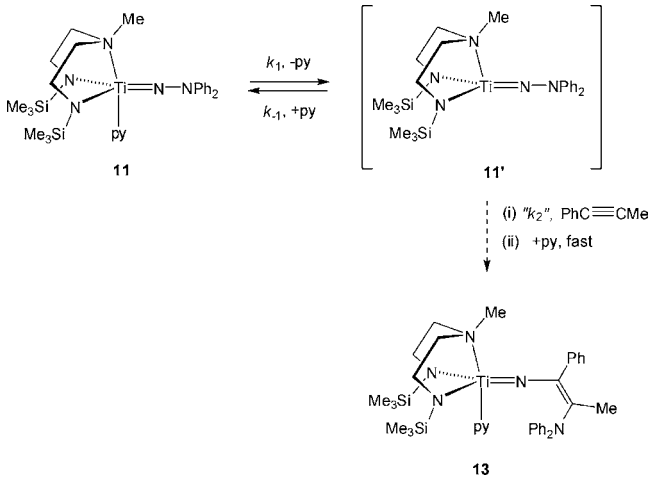

analogous to mechanisms previously established[75,82] for the cycloaddition reactions of the base-stabilized imides $Cp_2Zr(NR)(L)$ or $Ti(N_2{}^{R'}N^{py})(NR)(py)$ (R = $SiMe_3$ or Xyl) with alkynes. Scheme 1 predicts that, in the presence of an excess of alkyne, the rates of reaction should follow pseudo-first-order kinetics according to eq 5 where k_{obs} is given by eq 6. The linear double-reciprocal plot is consistent with eq 7.

$$\text{Rate} = k_{obs}[\mathbf{11}] \tag{5}$$

$$k_{obs} = \frac{k_1 k_2[\text{PhCCMe}]}{k_2[\text{PhCCMe}] + k_{-1}[\text{py}]} \tag{6}$$

$$\frac{1}{k_{obs}} = \frac{1}{k_1} + \frac{k_{-1}[\text{py}]}{k_1 k_2} \times \frac{1}{[\text{PhCCMe}]} \tag{7}$$

As a test of eq 6 the DMAP analogue of **11**, namely $Ti(N_2N^{Me})(NNPh_2)(DMAP)$ (**21**) was prepared. DMAP is a stronger donor than pyridine and, in agreement with Scheme 1 and eq 6, compound **21** reacted with PhCCMe significantly more slowly than **11** to form the corresponding insertion product $Ti(N_2N^{Me})\{NC(Ph)C(Me)NPh_2\}(DMAP)$ (**22**, eq 3). When followed by ^{1}H NMR spectroscopy in toluene-d_8, the reaction between **21** and PhCCMe (20 equiv) had $t_{1/2} = 3$ h at 0 °C whereas for **11** $t_{1/2} = 41$ min at −26 °C under otherwise identical conditions.

Addition of 1 or 2 equiv of pyridine to a mixture of **11** and PhCCMe in toluene-d_8 also significantly decreased the rate of the insertion reaction, consistent with Scheme 1 and eq 6. However, a control experiment in toluene-d_8 showed that **11** on its own reacts with added pyridine to form a fluxional new species (**23**) with apparent C_s symmetry, the amount of which increases with decreasing temperature. Compound **23** is probably the bis(pyridine) adduct $Ti(N_2N^{Me})(NNPh_2)(py)_2$ (Scheme 2). Although the decreased rate of reaction of **11** with PhCCMe in the presence of added pyridine is consistent with a reciprocal dependence on k_{-1}[py] (eqs 5 and 6), it is also consistent with partial trapping (to some unknown extent) of **11** to form unreactive **23** which exists in a rapid dynamic equilibrium with **11** at −30 °C (separate resonances for **11**, **23** and py are only observed below −50 °C).

Although **23** is labile and cannot be isolated, the 2,2′-bipyridyl analogue $Ti(N_2N^{Me})(NNPh_2)(bipy)$ (**24**) was readily prepared and structurally characterized (see the SI). The geometry at Ti(1) is approximately octahedral with the $NNPh_2$ positioned *trans* to the NMe donor, as indicated in Scheme 2. Compound **24** did not react at all with PhCCMe or C_6F_5CCMe at room temperature over the course of several days.

The reaction between **11** and PhCCMe (20 equiv) was followed at five different temperatures between −16 and −35 °C. The linear pseudo-first-order log plots and corresponding Eyring analysis ($\ln(k_{obs}/T)$ vs $1/T$) are shown in the SI. The derived activation enthalpy and entropy values for the rate-limiting barrier on the reaction coordinate **11** + PhCCMe → **13** are $\Delta H^{\ddagger} = 18.8(4)$ kcal mol^{-1} and $\Delta S^{\ddagger} = 1(1)$ cal mol^{-1} K^{-1} ($\Delta G^{\ddagger}_{298} = 18.5(7)$ kcal mol^{-1}). The negligible $\Delta S^{\ddagger}$ term implies that the rate limiting step involves neither ligand loss (e.g., **11** → **11′** + py (k_1, Scheme 1)) nor ligand gain.[83] The highest activation barrier within the "k_2" process in Scheme 1 is therefore likely to be an intramolecular rearrangement.

As shown in eq 3, compound **11** also reacted with a series of *p*-substituted alkynes $(4\text{-}C_6H_4X)CCMe$ (X = Me, ^{t}Bu, OMe, CF_3) to form the corresponding $N_\alpha{-}N_\beta$ insertion products **14**−**17**. To gain insight into the rate-limiting "k_2" step, all four reactions were followed at −26 °C in toluene-d_8 with 20 equiv alkyne. The reactions for X = Me, ^{t}Bu, and OMe showed the same behavior as for PhCCMe (i.e., X = H, Figure 4, top), whereas $(4\text{-}C_6H_4CF_3)CCMe$ entered a different kinetic regime which is discussed below. The pseudo-first-order rate constants (k_{obs}) for X = H, Me, ^{t}Bu, OMe are listed in Table 1 along

(82) Lee, S. Y.; Bergman, R. G. *Tetrahedron* **1995**, *51*, 4255.

(83) Jordan, R. B. *Reaction Mechanisms of Inorganic and Organometallic Systems*; Oxford University Press: Oxford, 1998.

Scheme 2. Reactions of **11** with Pyridine and bipy

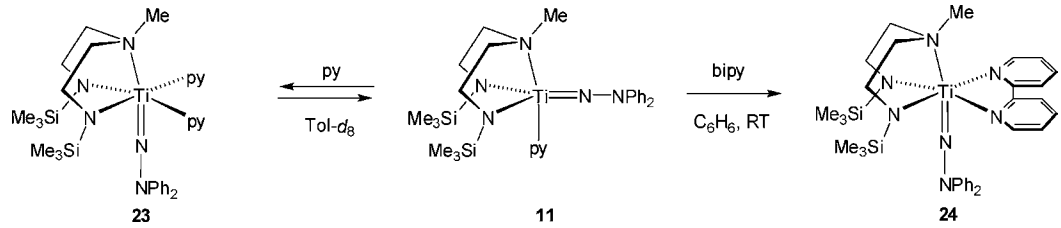

Table 1. Rate Constants (k_{obs}) for the $N_\alpha-N_\beta$ Insertion Reactions of Ti(N_2N^{Me})($NNPh_2$)(py) (**11**) with (4-C_6H_4X)CCMe (20 equiv, X = H, Me, ^{t}Bu, or OMe) at −26 °C in Toluene-d_8; σ_p is the Substituent Constant; $\Delta G^‡$ is the Gibbs Free Energy (kcal mol^{-1}) of the Transition State for $N_\alpha-N_\beta$ Cleavage According to DFT Using the Model Hydrazide **A1** (See the Computational Studies Section for Further Details)

X	$k_{obs} \times 10^4$ (s^{-1})	σ_p	$\Delta G^‡$ (kcal mol^{-1})
H	2.79(1)	0.00	20.7
Me	3.85(2)	−0.17	20.4
^{t}Bu	3.90(4)	−0.20	20.0
OMe	4.42(2)	−0.27	19.6

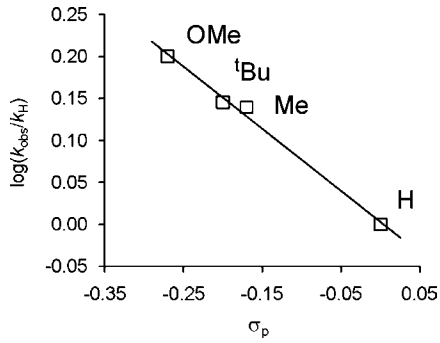

Figure 6. Plot of $\log(k_{obs}/k_H)$ vs σ_p for the reactions of Ti(N_2N^{Me})($NNPh_2$)(py) (**11**) with (4-C_6H_4X)CCMe (20 equiv, X = H, Me, ^{t}Bu, OMe) at −26 °C in toluene-d_8. The best-fit line shown had $r^2 = 0.992$ giving $\rho = -0.74(5)$ and k_H is k_{obs} for X = H.

with the corresponding Hammett substituent constants, σ_p.[84] Table 1 also gives the Gibbs free energy ($\Delta G^‡$, kcal mol^{-1}) of the DFT calculated transition state for $N_\alpha-N_\beta$ cleavage which will be discussed in the Computational Studies section below.

The k_{obs} data clearly show that the rate of reaction increases as the *para*-X substituent becomes more electron-releasing. The Hammett plot of $\log(k_{obs}/k_H)$ vs σ_p (Figure 6) gave a good agreement and yielded a reaction constant, ρ, of −0.74(5). A plot of $\log(k_{obs}/k_H)$ vs σ_p^+ gave a poorer fit ($r^2 = 0.778$). The negative value of ρ is indicative of the development of positive charge (or disappearance of negative charge) at the ArC alkyne carbon in the transition state for alkyne insertion into $N_\alpha-N_\beta$. We will return to this point later on in the Computational Studies section.

As mentioned above, the more electron-deficient alkynes Ar^FCCMe (Ar^F = 4-$C_6H_4CF_3$ or C_6F_5) also undergo $N_\alpha-N_\beta$ insertion reactions with **11**, forming **17** and **18** (eq 3). However, when these reactions were monitored in toluene-d_8 at low temperature, a different kinetic regime was observed. In each instance, at temperatures between −40 and −30 °C, equilibrium mixtures were formed (Scheme 3) consisting of **11** (and/or its bis(pyridine) homologue, **23**), Ar^FCCMe, free pyridine, and new species characterized as the cycloaddition products Ti(N_2N^{Me}){N(NPh_2)C(Me)CAr^F} (Ar^F = 4-$C_6H_4CF_3$ (**25**) or C_6F_5 (**26**)) on the basis of the similarity of their NMR data to those of the isolated and fully authenticated metallacycles Ti(N_2N^{py}){N(NPh_2)C(Me)CAr^F} (Ar^F = 4-$C_6H_4CF_3$ (**3**) or C_6F_5 (**4**)). On warming, these first-formed equilibrium mixtures quantitatively converted to the final insertion products **17** and **18**, respectively (Scheme 3). Single crystals of **18** were of poor quality, but allowed the connectivity to be established (see the SI), confirming that shown in Scheme 3.

Due to the experimental uncertainties concerning the extent to which **11** (or indeed **17** or **18**) trap (or are trapped by) the free pyridine generated by formation of the intermediates **25** or **26** (whose relative concentration varies throughout the reaction), we have not quantitatively modeled the new kinetic regime. However, it is qualitatively clear from the rate of evolution of **17** (Figure 7) that the overall reaction **11** with (4-$C_6H_4CF_3$)CCMe takes significantly longer than with (4-C_6H_4X)CCMe (X = H, Me, ^{t}Bu, OMe; $t_{1/2}$ = ∼26−41 min) under otherwise identical conditions.

The reactions of **11** with Ar^FCCMe are reminiscent of that between Ti(N_2N^{py})($NNPh_2$)(py) (**1**) and PhCCMe. In each case a first-formed equilibrium mixture of starting hydrazide and [2 + 2] cycloaddition product goes on to form a $N_\alpha-N_\beta$ insertion product. For both **1** and **11**, it appears that the electron-withdrawing aryl ring substituents in Ar^FCCMe stabilize the resultant metallacycles, whereas electron-donating groups (*cf.* Figure 6) promote $N_\alpha-N_\beta$ bond insertion. Although Figure 7 suggests that metallacycles might lie on the reaction coordinate from **1** and **11** to the insertion products, such species are not observed in the majority of instances (*cf.* Figure 4 and the reactions of **11** with (4-C_6H_4X)CCMe (X = H, Me, ^{t}Bu, OMe)). To gain further insight into this chemistry we carried out a comprehensive series of DFT studies as described below.

Scheme 3. Reaction of Ti(N_2N^{Me})($NNPh_2$)(py) (**11**) with Ar^FCCMe (Ar^F = 4-$C_6H_4CF_3$ or C_6F_5)

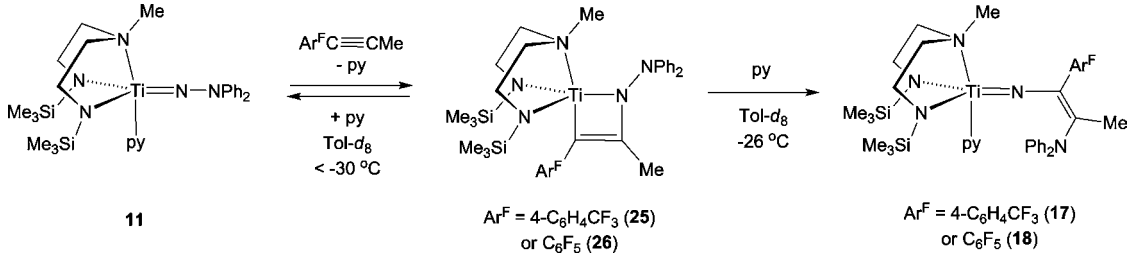

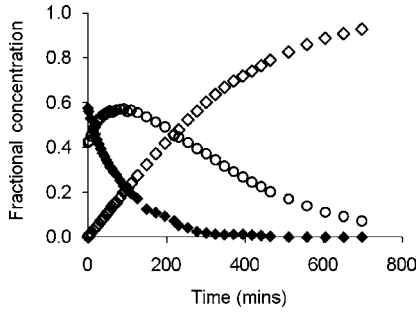

Figure 7. Decay and/or evolution with time of titanium species involved in the reaction of Ti(N_2N^{Me})($NNPh_2$)(py) (**11**, filled diamonds) with (4-$C_6H_4CF_3$)CCMe (20 equiv) at −26 °C. Other species are: Ti(N_2N^{Me}){NC(4-$C_6H_4CF_3$)C(Me)NPh_2} (**17**, hollow diamonds) and Ti(N_2N^{Me}){N(NPh_2)C-(Me)C(4-$C_6H_4CF_3$)} (**25**, hollow circles).

Computational Studies

Mechanism of Alkyne Insertion into $N_\alpha-N_\beta$. DFT(B3PW91) calculations were carried out using Ti($N_2^{SiH_3}N^{Me}$)(NNR_2)(py) (R = Me (**A1**) or Ph (**B1**)) as models for **11**, and Ti($N_2^{SiH_3}N^{py}$)($NNMe_2$)(py) (**C1**) as a model for **1**. In all three, the $SiMe_3$ groups of N_2N^R (R = Me or py) have been replaced by SiH_3, and in **A1** and **C1** Ti=$NNPh_2$ is modeled by Ti=$NNMe_2$ for computational efficiency. The results obtained with **B1** are similar to those with **A1** and are presented in the SI. To establish the basic electronic features of the mechanism, MeCCMe (2-butyne) was considered as the reacting alkyne.

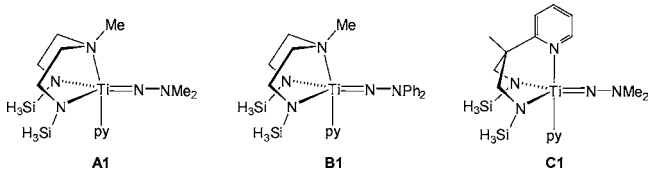

Scheme 4. Two Potential Mechanisms for Alkyne Insertion into the $N_\alpha-N_\beta$ Bond of the Hydrazide Ligand in **1** or **11**. [Ti] = Ti(N_2N^{py}) or Ti(N_2N^{Me})

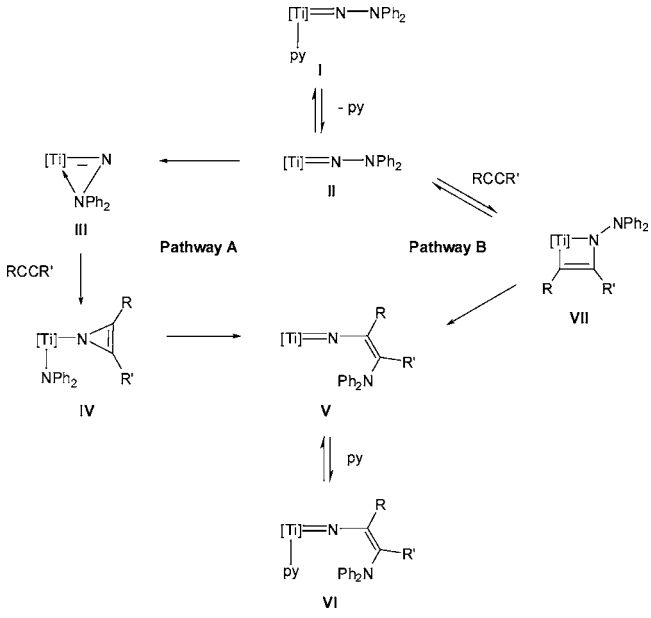

Scheme 4 shows the two mechanisms (designated Pathways A and B) we have investigated for the $N_\alpha-N_\beta$ insertion reactions of **1** and **11**. Pathway A has recently been proposed by Mindiola

Scheme 5. Gibbs Free Energy (kcal mol^{-1}) Profile for MeCCMe Insertion into the $N_\alpha-N_\beta$ Bond of Ti($N_2^{SiH_3}N^{Me}$)($NNMe_2$)(py) (**A1**) along Pathway A; [Ti] = Ti($N_2^{SiH_3}N^{Me}$)

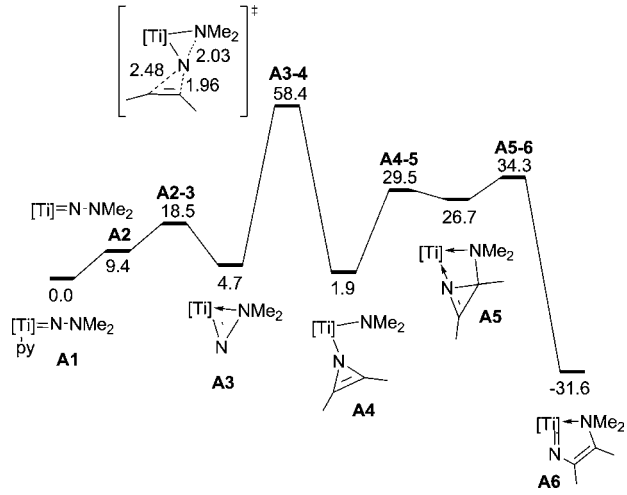

following our initial communication on the insertion reaction of **11** with PhCCMe.[3] In this mechanism, loss of pyridine from **I** forms an η^2-hydrazide **III** *via* base-free **II**. This intermediate was proposed to then undergo [2 + 1] cycloaddition at N_α with RCCR′ forming an N-metalated azirine intermediate (**IV**) with concomitant $N_\alpha-N_\beta$ bond breaking. Ring-opening of the azirine *via* NPh_2 group transfer from Ti back to CR′ affords the four-coordinate insertion product **V** which is then trapped by pyridine giving **VI**. Gade has also proposed a similar η^2-hydrazido intermediate in the $N_\alpha-N_\beta$ cleavage reaction of Zr(N_2*N^{py})($NNPh_2$)(py) with isocyanides (N_2*N^{py} = (2-NC_5H_4)CMe($CH_2NSiMe_2{}^tBu$)$_2$).[42] Mindiola's mechanism is consistent with our experimental evidence for a pyridine-free intermediate being formed before reaction with the alkyne. Furthermore, if the intramolecular transformation **IV** → **V** were the rate-limiting step, then the experimental near-zero entropy of activation for **11** + PhCCMe → **13** could likewise be consistent with Pathway A. Finally, Gade has described how a version of **III** derived from M(N_2*N^{py})($NNPh_2$)(py) (M = Zr, Hf) can be trapped by electrophilic addition of $B(C_6F_5)_3$ to N_α.[33] Therefore, DFT calculations were used to determine the details of the mechanism along Pathway A and the nature of the rate-limiting step.

The DFT Gibbs free energy profile along Pathway A for **A1** reacting with MeCCMe is shown in Scheme 5. Formation of a vacant site (in **A2**) by pyridine dissociation is unfavorable by ΔG = 9.4 kcal mol^{-1}. Dissociation of DMAP was calculated to be even more difficult (ΔG = 11.8 kcal mol^{-1}), as expected. The calculated ΔG value for pyridine loss from **A1** compares well with those measured experimentally for some imidotitanium complexes.[85] The activation barrier for dissociation of a ligand is not easy to estimate computationally as often no transition state (TS) can be located for such a process. However, on the assumption[86] that the activation barrier $\Delta G^{\ddagger}$ is essentially the enthalpy cost of breaking the metal−ligand bond (i.e., $\Delta G^{\ddagger} \approx \Delta H$), the barriers (i.e., $\Delta G^{\ddagger}$) for pyridine and DMAP dissociation are 21.9 and 24.6 kcal mol^{-1}, respectively. These values

(84) Hansch, C.; Leo, A.; Taft, R. W. *Chem. Rev.* **1991**, *91*, 165.
(85) Stewart, P. J.; Blake, A. J.; Mountford, P. *Inorg. Chem.* **1997**, *36*, 3616.
(86) Hartwig, J. F.; Cook, K. S.; Hapke, M.; Incarvito, C. D.; Fan, Y.; Webster, C. E.; Hall, M. B. *J. Am. Chem. Soc.* **2005**, *127*, 2538.

Scheme 6. Gibbs Free Energy (kcal mol^{-1}) Profile for MeCCMe Insertion into the $N_\alpha-N_\beta$ Bond of Ti($N_2^{SiH_3}N^{Me}$)(NNMe$_2$)(py) (**A1**) along Pathway B[a])

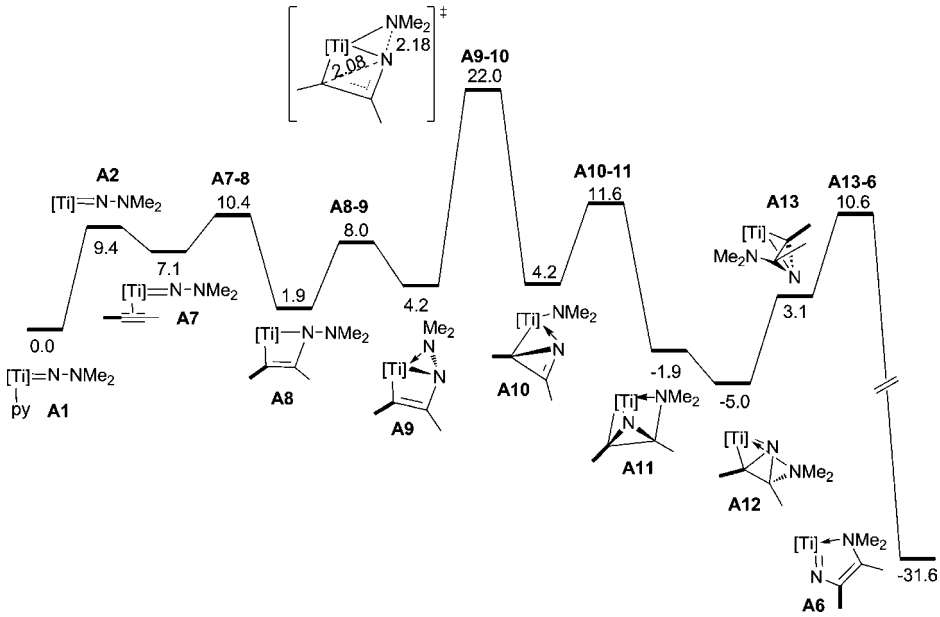

[a] The bond shown in bold for the alkyne is to help the reader trace the fate of the Ti-bound CMe group in **A8**. [Ti] = Ti($N_2^{SiH_3}N^{Me}$).

constitute an upper estimate of the actual activation barriers. The larger value for DMAP is in agreement with the lower rate of reaction observed with **21** compared to that with **11**. Experimentally determined $\Delta G^{\ddagger}$ values for pyridine loss from certain 5- and 6-coordinate imidotitanium complexes (including a homologue of **1**) have been reported to be ~15 kcal mol^{-1}.[75,85]

From **A2** (Scheme 5) coordination of N_β yields two potential intermediates: **A3**, where N_α shifts to the vacant site and N_β coordinates in the equatorial plane; and **A3b**, where N_β coordinates directly to the vacant site as indicated for species **III**, Scheme 4. **A3** is 8.7 kcal mol^{-1} more stable than **A3b**, and only for the former could a TS for $N_\alpha-N_\beta$ bond breaking be located. Formation of **A3** from **A2** is exergonic (−4.7 kcal mol^{-1}) and proceeds with a low activation barrier (9.1 kcal mol^{-1} relative to **A2**).

The crucial step in Pathway A is the formation of the N-metalated azirine **IV**. This is modeled as **A4** in Scheme 5, formed by reaction of **A3** with MeCCMe. As proposed by Mindiola, this reaction is a [2 + 1] cycloaddition between the alkyne and N_α of a bent hydrazido ligand. The cycloaddition occurs with concomitant $N_\alpha-N_\beta$ bond cleavage as illustrated by the lengthening of the $N_\alpha-N_\beta$ bond from 1.41 Å in **A3** to 2.03 Å in the transition state **A3**−**4**. However, even though the transformation from **A3** to **A4** is slightly exergonic (−2.8 kcal mol^{-1}), the associated activation barrier is prohibitively high (53.7 kcal mol^{-1} at 298 K). Frontier orbital analysis shows that this is because N_α in this type of η^2-hydrazide species is nucleophilic in nature, not electrophilic.[33] **A3**−**4** is a late transition state for $N_\alpha-N_\beta$ cleavage *with little C*−N_α *bond-forming character* (C−N_α = 1.96 and 2.48 Å in **A3**−**4**), thus explaining the high activation barrier (see Figure S4 in the SI for the geometry of **A3**−**4**).

From **A4**, nucleophilic transfer of the Ti-bound NMe$_2$ group to an azirine ring carbon atom affords **A5**, and subsequent ring-opening leads to the *Z* aza-allyl intermediate **A6** in an energetically favorable process. Upon decoordination of the chelating NMe$_2$ group, the vinyl imido shifts to the equatorial position, and coordination of pyridine yields finally the insertion product (not shown in Scheme 5).

The high computed barrier **A3**−**4** for Pathway A and the bimolecular nature of the rate-determining step suggest that the $N_\alpha-N_\beta$ insertion reactions of **1** and **11** follow another mechanism. This is designated Pathway B in Scheme 4 and assumes that azatitanacyclobutenes of the type **VII** play an *active role* in the formation of **V** and **VI**, rather than being separate species unconnected with $N_\alpha-N_\beta$ insertion. While they are not always observed, metallacycles (e.g., **2** (eq 1) and **25** and **26** (Scheme 3)) have sometimes been seen in reaction mixtures that also give rise to $N_\alpha-N_\beta$ insertion. DFT calculations of Pathway B were therefore carried out also on the model system **A1** (Scheme 6). This pathway would constitute a way to insert an alkyne into the $N_\alpha-N_\beta$ bond after pyridine dissociation and so could be in agreement with the experimental kinetic studies, providing the rate-determining step occurs *after* the [2 + 2] cycloaddition of the alkyne. A pathway starting by coordination of the alkyne *before* the pyridine dissociates was searched for, but no stable intermediate could be located on the potential energy surface. Therefore, only Pathway B, initiated by pyridine dissociation, will be described.

The vacant site in **A2**, created by pyridine decoordination, is a potential site for alkyne coordination. Coordination of MeCCMe (forming **A7**) is less favorable than formation of the η^2-hydrazide **A3** (Scheme 5), partly due to the loss of translational entropy in the former case. Nonetheless, [2 + 2] cycloaddition from **A7** to form the azatitanacyclobutene **A8** occurs readily with a low barrier (3.3 kcal mol^{-1}) and is thermodynamically competitive with **A1** (ΔG = 1.9 kcal mol^{-1}). From **A8**, intramolecular coordination of $N_\beta Me_2$ is facile and proceeds with a low barrier (6.1 kcal mol^{-1}) to yield the key intermediate **A9**, lying only 4.2 kcal mol^{-1} above the separated reactants **A1** and MeCCMe. The $N_\alpha-N_\beta$ bond-breaking step proceeds through **A9**−**10**, yielding the C,N-metalated azirine **A10** in a thermoneutral reaction. The activation barrier is only 17.8 kcal mol^{-1} above **A9**, and is 36.4 kcal mol^{-1} less than the $N_\alpha-N_\beta$ bond

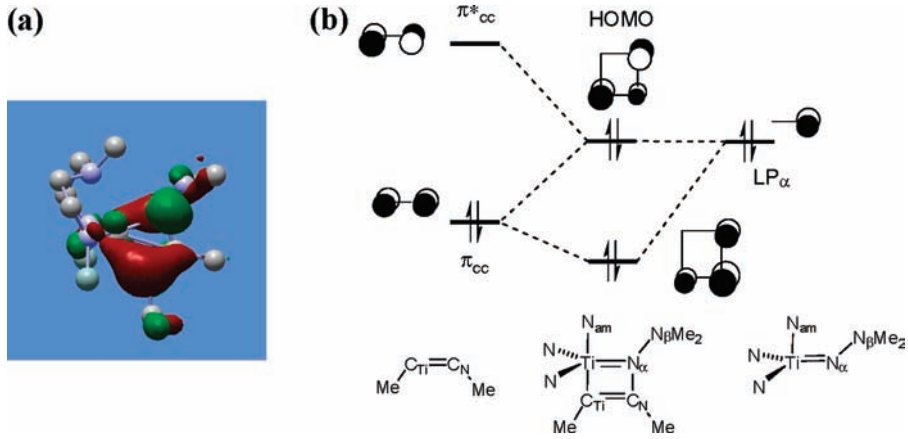

Figure 8. (a) HOMO of **A8**. (b) Schematic MO diagram for the π interactions within the 4-membered metallacycle

cleavage through **A3**−**4** (Scheme 5). This is because $N_\alpha-N_\beta$ bond breaking in **A9**−**10** is coupled with $C-N_\alpha$ bond forming, thus lowering the activation barrier of the process. A detailed discussion of the sequence **A8** → **A9** → **A9**−**10** and the electronic structures of these species is given later on.

From **A10** the reaction proceeds *via* exergonic nucleophilic attack of the Ti-bound NMe_2 group on the azirine ring to form **A11** with a low activation barrier. Two other isomers (**A12** and **A13**), differing in the relative orientations of N_α and N_β with respect to the $N_2^{SiH_3}N^{Me}$ ligand, have been located on the potential energy surface. The activation barrier for the isomerization of **A11** to **A12** (through **A11**−**12**, not shown in Scheme 6) is only 5.5 kcal mol^{-1}. Each of these three intermediates can lead to the cleavage of the $C-N_\alpha$ bond to form **A6**. However, the TS with the lowest energy is **A13**−**6** originating from **A13**, and the corresponding activation barrier is 7.5 kcal mol^{-1}. Overall, the net $N_\alpha-N_\beta$ *insertion* reaction is mechanistically a *Ti*=N_α *cycloaddition* followed by an N_α *atom migration* process.

Comparison of the DFT computed Pathways A and B (Schemes 5 and 6) shows clearly that the latter is preferred. From **A1**, the activation barrier to overcome along Pathway A (**A3**−**4**) is 58.4 kcal mol^{-1}, whereas the highest point along Pathway B (**A9**−**10**) is only 22.0 kcal mol^{-1}. The latter value is in much better agreement with the experimental activation barrier determined for PhCCMe reacting with **11** ($\Delta G^{\ddagger}_{298} = 18.5(7)$ kcal mol^{-1}). Moreover, whereas in Pathway A the rate-determining step is bimolecular, in Pathway B it is intramolecular. The experimental low value for $\Delta S^{\ddagger}$ (1(1) cal mol^{-1} K^{-1}) is in better agreement with an intramolecular rate-determining step, lending further support to Pathway B as the most likely reaction mechanism. The relevant calculated $\Delta S^{\ddagger}$ values are −41.3 cal mol^{-1} K^{-1} (**A3**−**4**) and 4 cal mol^{-1} K^{-1} (**A9**−**10**), the latter being consistent with experimental measurement.

Origins of Regioselectivity for $N_\alpha-N_\beta$ Insertion. When **1** and **11** undergo $N_\alpha-N_\beta$ insertion with unsymmetrical alkynes ArCCMe, the products always have CAr bound to Ti=N_α of the originating hydrazide and CMe bound to $N_\beta Ph_2$ (eqs 2−4). In the corresponding metallacycles, however, it is always CMe which is bound to N_α (eqs 1 and 3). This is fully consistent with Pathway B. As illustrated by a bold bond for one of the alkyne C−Me groups in Scheme 6, it is the regiochemistry of the *cycloaddition product* which determines that of the insertion product. That is to say, the alkyne carbon initially bonded to Ti in the metallacycle **A8** ends up bonded to N_α in the insertion product **A6**, and the alkyne substituents are mutually *cis* as found exclusively by experiment.

To fully understand the origins of this critical regiochemical preference, we have analyzed the electronic structure of the azatitanacyclobutene **A8**. The HOMO of this complex (Figure 8a) results from the stabilization of the 4-electron repulsion between the lone pair on N_α (LP_α) and the filled π_{cc} MO by the vacant π^*_{cc} MO (Figure 8b). As a consequence of the mixing between these three orbitals, the HOMO is essentially based on N_α and the carbon atom bonded to Ti (denoted C_{Ti}).

With regard to regiochemical preferences, substitution of a methyl group in **A8** by any group "X" that would decrease the 4-electron repulsion would result in a more stable metallacycle. For example, an electron-withdrawing group X would increase the effective electronegativity of the carbon to which it is attached. This would in turn result in a stabilization of both π_{cc} and π^*_{cc} and also in a polarization of π_{cc} toward the X-substituted carbon atom. The schematic MO diagram in Figure 8b indicates that the best situation corresponds to the regioisomer with the electron-withdrawing X bonded to C_{Ti}. In that case, the destabilizing overlap between LP_α and π_{cc} would be reduced and the favorable overlap between LP_α and π^*_{cc} would be increased; both factors combine to lower the energy of the HOMO.

These arguments, based on the effective electronegativity of the alkyne carbon atoms, essentially involve the σ-acceptor properties of the X group. However, π-effects must also be considered. For example, it is well-known[87] that the HOMO of an alkene moiety $XC(R)=CR_2$ is more strongly developed on the $\underline{C}R_2$ carbon when X is a π-donor. In the case of an azatitanacyclobutene of the type **A8**, the best arrangement to minimize repulsion between π_{cc} and LP_α would be the regioisomer with X bonded to C_N. For σ-accepting but π-donating groups the preferred product will come from a balance of the two effects as each favors a different regioisomer. For X groups which are both σ- and π-accepting, the two contributions favor the same regioisomer, with X bonded to C_{Ti}.

Equation 8 shows the possible products **Ar(Ti)_R** and **Ar(N)_R** that can be formed between **A1** and ArCCR (Ar = Ph or substituted phenyl; R = Me or H). These are homologues of **A8**, formed from **A1** and MeCCMe for which $\Delta G = 1.9$ kcal mol^{-1} (Scheme 6). Changing from MeCCMe to PhCCMe gives two possible regioisomers, **Ph(Ti)_Me** and **Ph(N)_Me** for which $\Delta G = 1.3$ kcal mol^{-1} and 6.7 kcal mol^{-1}, respectively. The increased stability of **Ph(Ti)_Me** compared to **A8** ($\Delta\Delta G$

(87) Nguyen, T. A. *Frontier Orbitals: A Practical Manual*; John Wiley & Sons: Chichester, 2007.

Table 2. Gibbs Free Energies (ΔG, kcal mol^{-1}) for the Cycloaddition Products **Ar(Ti)_R** (see eq 8) Expressed Relative to Separated **A1** and ArCCR[a]

Ar	R	ΔG
Ph	H	−7.5
Ph	Me	1.3
4-$C_6H_4CF_3$	Me	−0.7
C_6F_5	Me	−1.6
4-$C_6H_4{}^t$Bu	Me	1.3
4-C_6H_4OMe	Me	1.4

[a] The cycloaddition product formed with MeCCMe (**A8**) has ΔG = 1.9 kcal mol^{-1}.

= −0.6 kcal mol^{-1}) is in agreement with a larger effective electronegativity at an sp^2 hybridized carbon atom (*ipso*-Ph) compared to an sp^3 hybridized one (Me). The decreased stability of **Ph(N)_Me** with respect to both **A8** ($\Delta\Delta G$ = +4.8 kcal mol^{-1}) and **Ph(Ti)_Me** ($\Delta\Delta G$ = +5.4 kcal mol^{-1}) indicates that Ph behaves as a π-accepting group in the azametallacycles. Consistent with this, the C−Ph bond in **Ph(Ti)_Me** (1.459 Å) is shorter than that in **Ph(N)_Me** (1.495 Å) as a result of better π conjugation. Shorter C−N_α and longer C═C bonds in **Ph(Ti)_Me** compared to **Ph(N)_Me** are also consistent with this model.

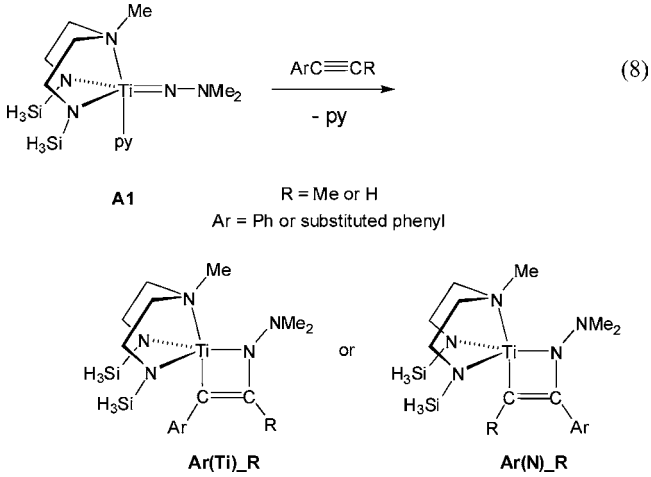

(8)

Changing from PhCCMe to the terminal alkyne PhCCH stabilizes both regioisomers relative to PhCCMe and MeCCMe. For **Ph(Ti)_H** ΔG = −7.5 kcal mol^{-1} and for **Ph(N)_H** ΔG = −1.9 kcal mol^{-1}. This is because H is less electron-releasing than Me, but Ph is more electron-accepting. Again the regioisomer with Ph bonded to C_{Ti} is very strongly favored by ~10^4 in terms of an equilibrium between the two. Focusing on this regioisomer, we also calculated ΔG for forming **Ar(Ti)_Me** from **A1** and experimentally relevant *para*-substituted alkynes, namely ArCCMe (Ar = C_6F_5 or 4-C_6H_4X with X = ^{t}Bu, OMe or CF_3). The results are given in Table 2 together with those for the other alkynes and are globally consistent with the bonding model introduced above. Strongly σ-accepting groups (Ar = 4-$C_6H_4CF_3$ (ΔG = −0.7 kcal mol^{-1}) or C_6F_5 (ΔG = −1.6 kcal mol^{-1})) stabilize **Ar(Ti)_Me** compared to the compounds where Ar = Ph or 4-$C_6H_4{}^t$Bu (ΔG = 1.3 kcal mol^{-1}). Interestingly, although the strongly π-donating *para* substituent OMe should in principle destabilize **Ar(Ti)_Me** (see above), the competing inductive and mesomeric influences of σ acceptor (−I) and π donor (+M) effects, respectively, lead to a product of only slightly lower stability (ΔG = 1.4 kcal mol^{-1}) than when Ar = Ph or 4-$C_6H_4{}^t$Bu.

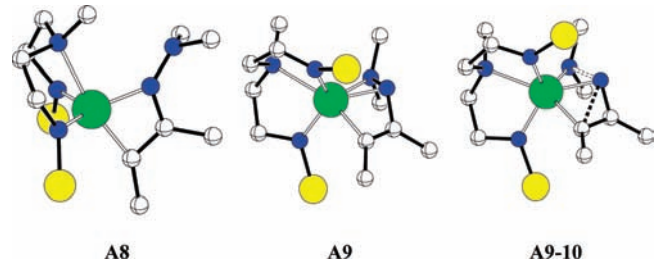

Figure 9. Optimized geometries for the azatitanacyclobutene **A8**, the $N_\beta Me_2$-chelated intermediate **A9**, and the TS for N_α−N_β cleavage (**A9**−**10**). H atoms have been omitted for clarity.

The DFT results are fully consistent with the experimental data. For example, **1** forms more stable [2 + 2] cycloaddition products with PhCCH than with PhCCMe, and none at all with MeCCMe; the metallacycles are more stable with electron-withdrawing Ar groups for both **1** and **11**; the only regioisomers observed are with Ar bound to C_{Ti}. Furthermore, when Ar is bound to C_{Ti} in **Ar(Ti)_Me** (i.e., at the bold bond in **A8** in Scheme 6) the product of the insertion reaction has precisely the geometry of the compounds observed experimentally.

Understanding the N_α−N_β Bond-Cleavage Step. The ground-state electronic preference of the azatitanacyclobutenes, which ultimately control the *regiochemistry* of the N_α−N_β insertion reaction, is for *electron-withdrawing* alkyne substituents, ideally attached to C_{Ti}. However, the experimental kinetic data (Table 1, Figure 6) suggest that *overall rates* of the insertion reaction are favored by *electron-releasing* alkyne substituents. At first sight, the factors that control the stability of the metallacycle are not necessarily the same as those governing the transition state for N_α−N_β cleavage. We therefore examined in further detail the rate-determining N_α−N_β breaking process for RCCMe (R = Me or Ar).

In the reaction of **A1** with MeCCMe (Scheme 6), cleavage of the N_α−N_β bond is effective in two steps from the azatitanacyclobutene **A8**. First, coordination of $N_\beta Me_2$ to Ti forms **A9**, and then N_α−N_β cleavage occurs through the transition state **A9**−**10** to form **A10**. This last step constitutes the rate-determining step of the entire alkyne insertion reaction. The geometries of the three critical extrema (**A8**, **A9**, and **A9**−**10**) are shown in Figure 9.

The coordination of $N_\beta Me_2$ induces a deformation of the 4-membered ring in the metallacycle **A8**. In **A9**, N_β is coplanar with Ti and the two carbon atoms (N_β−Ti−C_{Ti}−C_N = 1.3°), while N_α is situated above that plane. Ti−N_β is longer than Ti−C_{Ti} (2.193 Å vs 2.068 Å). The N_β−Ti−C_{Ti} angle is 101°, and N_α is situated between C_N and N_β (N_α−C_N = 1.444 Å, N_α−N_β = 1.454 Å). The coordination of $N_\beta Me_2$ results in a slight activation of the N_α−N_β bond (1.401 Å in **A8**, 1.454 Å in **A9**), and has positioned the N_α−N_β axis above the plane containing the C═C π bond.

The geometry of **A9** is perfectly adapted for nucleophilic attack from the π density polarized toward C_{Ti} into the σ^*(N_α−N_β) antibonding MO. Indeed, the geometry of the transition state **A9**−**10** confirms the description of the N_α−N_β cleavage as effectively a nucleophilic attack of C_{Ti} on N_α. The $C_{Ti}\cdots N_\alpha$ distance decreases by ~0.2 Å (from 2.268 Å in **A9** to 2.077 Å in **A9**−**10**) while the $N_\alpha\cdots N_\beta$ distance increases by ~0.7 Å (from 1.454 Å in **A9** to 2.185 Å in **A9**−**10**). These variations are accompanied by an increase of the N_β−Ti−C_{Ti} angle to 117°, a lengthening of Ti−C_{Ti} to 2.127 Å, and a shortening of Ti−N_β to 2.068 Å. To increase the nucleophilic

Scheme 7. Gibbs Free Energy (kcal mol^{-1}) Profile for MeCCMe Insertion into the $N_\alpha-N_\beta$ Bond of Ti($N_2^{SiH_3N^{py}}$)($NNMe_2$)(py) (**C1**) along Pathway B

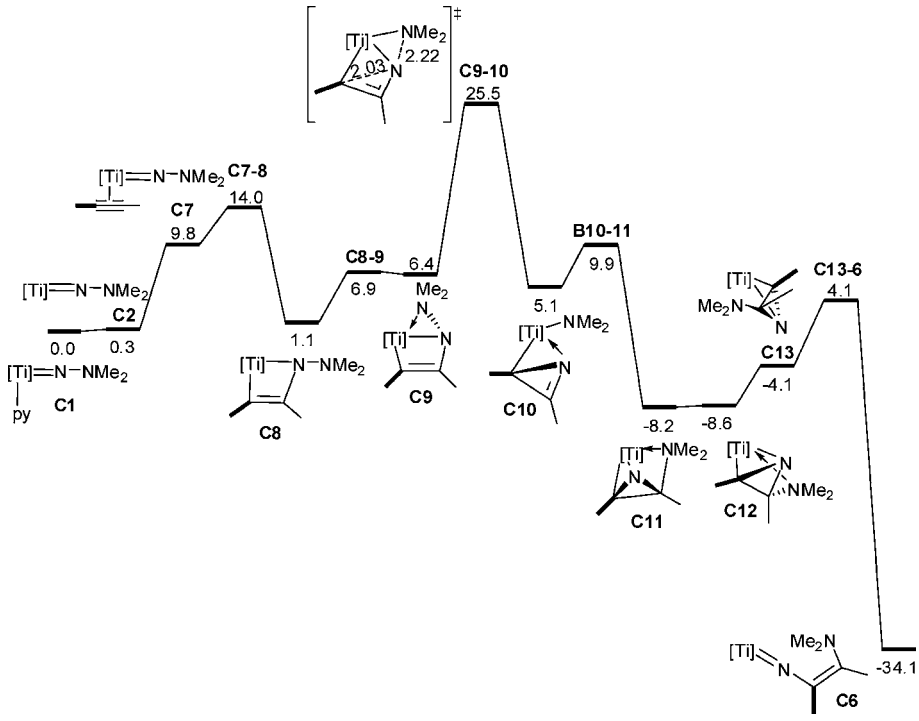

The bond shown in bold for the alkyne is to help the reader trace the fate of the Ti-bound CMe group in **C8**. [Ti] = Ti($N_2^{SiH_3Npy}$).

character at C_{Ti}, the C=C π bond is partially lost. This is illustrated by the increase in the Me$-C_{Ti}-C_N-$Me dihedral angle from 4.1° in **A9** to 33.2° in **A9**$-$**10** and lengthening of $C_{Ti}-C_N$ from 1.355 Å in **A9** to 1.383 Å in **A9**$-$**10**. The twist around the $C_{Ti}-C_N$ axis allows the formation of a $N_\alpha=C_N$ π bond, while preserving some lone pair character at C_{Ti}. The $N_\alpha-C_N$ bond distance shortens significantly in the transition state **A9**$-$**10** (1.444 Å in **A9**, 1.348 Å in **A9**$-$**10**). The relative low energy of **A9**$-$**10**, and hence the facile $N_\alpha-N_\beta$ bond cleavage, is the result of several stabilizing effects working cooperatively. The nucleophilic substitution at N_α of N_β by C_{Ti} is facilitated by the formation of stabilizing Ti$-NMe_2$ and $N_\alpha=C_N$ interactions. Any factor increasing the nucleophilicity at C_{Ti} is likely to lower the energy of the transition state.

The TS Gibbs free energies ($\Delta G^\ddagger$) for the $N_\alpha-N_\beta$ cleavage step (analogous to **A9**$-$**10** with MeCCMe) for the alkynes (4-C_6H_4X)CCMe (X = H, Me, ^{t}Bu, OMe) used in the Hammett study are listed in Table 1 alongside the experimental rate constants. The $\Delta G^\ddagger$ values for ArCCMe are all less than for MeCCMe itself (22.0 kcal mol^{-1}), in keeping with experimental observations that the reaction of **11** with MeCCMe is much slower than with PhCCMe. The $\Delta G^\ddagger$ values decrease in the order *para*-X = H > Me > ^{t}Bu > OMe, which is consistent with the ordering of the experimental rate constants (k_{obs} for *para*-X = H < Me < ^{t}Bu < OMe) and nucleophilic attack of C_{Ti} on N_α in the $N_\alpha-N_\beta$ breaking TS being promoted by electron-releasing *para*-substituents. $\Delta G^\ddagger$ for the reaction of (4-$C_6H_4CF_3$)CCMe with **A1** was calculated to be 21.7 kcal mol^{-1}, higher than for PhCCMe (20.7 kcal mol^{-1}) because the electron-withdrawing *para*-CF_3 group diminished the nucleophilicity of C_{Ti}. Note that $\Delta G^\ddagger$ for $N_\alpha-N_\beta$ cleavage starting from the less stable, alternative cycloaddition regioisomer **Ph(N)_Me** was 24.1 kcal mol^{-1}.

Consistent with the *para* substituent effects, we find that the NPA charge of C_{Ti} in **A8**, **A9**, and **A9**$-$**10** becomes more positive along the reaction coordinate ($-$0.473, $-$0.363, $-$0.187, respectively). An analogous trend was found for the corresponding species formed with PhCCMe ($-$0.506, $-$0.387, $-$0.232, respectively) but with the Ph group stabilizing a more negative charge at C_{Ti} at each stage as expected. The overall NPA charge of the Ph group also becomes more positive on going from the metallacycle **Ph(Ti)_Me** ($-$0.060) to the $N_\alpha-N_\beta$ breaking TS (+0.030), again consistent with the effects of electron-releasing ring substituents.

Taken together, the trends in the computed $\Delta G^\ddagger$ and experimental k_{obs} values, and the negative Hammett reaction constant ρ are consistent with $N_\alpha-N_\beta$ bond cleavage being caused by intramolecular nucleophilic attack of C_{Ti} on N_α. The form of the conversion vs time plot in Figure 7 is a consequence of enhanced ground-state stabilization of the metallacycle (*cf.* Table 2) and concomitant destabilization of the $N_\alpha-N_\beta$ cleavage TS by the electron-withdrawing 4-$C_6H_4CF_3$ group. The observed product regiochemistry with ArCCMe comes from both the relative stability of the precursor metallacycles and the associated transition states.

N_2N^{py} vs N_2N^{Me}: Influence of the Diamide-Amine Ligand Sets. Experimentally, there is a significant difference between the rates of the $N_\alpha-N_\beta$ insertion reaction for Ti(N_2N^{py})($NNPh_2$)(py) (**1**) and Ti(N_2N^{Me})($NNPh_2$)(py) (**11**). While the latter leads to PhCCMe insertion within ~5$-$10 min at room temperature, the former requires ~3 days (or heating at 60 °C for 3 h). In addition, alkyne cycloaddition products are readily isolated with **1**, whereas these were barely observable with **11**, and only at $-$30 °C or below (Scheme 3).

To probe these differences, the Gibbs free energy profile for the $N_\alpha-N_\beta$ insertion reaction along Pathway B (Scheme 4) for the model system Ti($N_2^{SiH_3N^{py}}$)($NNMe_2$)(py) (**C1**) has been calculated (Scheme 7). From **C1**, formation of a vacant site is almost thermoneutral (ΔG = 0.3 kcal mol^{-1}), and the activation barrier (12.1 kcal mol^{-1}) for pyridine dissociation is significantly reduced compared to that in **A1** (21.9 kcal mol^{-1}). The relative

stability of the base-free complex **C2** compared to that of **A2** is due to the higher *trans* influence of pyridyl (in $N_2^{SiH_3}N^{py}$) compared to that of NMe (in $N_2^{SiH_3}N^{Me}$) in the ground states of the adducts **C1** and **A1** (*cf.* Ti−N_{py} in **1** and **11** = 2.259(2) Å and 2.215(5) Å, respectively[34]) and the larger chelate ring size (6-membered vs 5-membered) of $N_2^{SiH_3}N^{py}$ between the amide nitrogens and the apical donor ($N_{pyridyl}$ or NMe). This allows better relative orientation of the various N_{amide} and N_α π-donors in **C2** leading to overall more effective stabilization of the unsaturation at Ti.[34] As a result, the metal center is less electrophilic in **C2** compared to that in **A2**, resulting in an endoergic coordination of MeCCMe (ΔG = 9.5 kcal mol^{-1}), whereas the coordination is exoergic in **A2** (ΔG = −2.3 kcal mol^{-1}).

From **C7**, [2 + 2] cycloaddition of MeCCMe to form **C8** is thermodynamically downhill (−8.7 kcal mol^{-1}) with a low activation barrier (4.2 kcal mol^{-1}). The metallacycle **C8** is only 1.1 kcal mol^{-1} above the starting materials and is ∼1 kcal mol^{-1} more stable than **A8**, in qualitative agreement with the relative ease of experimental observation of metallacycles for **1** vs **11**. From **C8**, the N_α−N_β bond cleavage is effective in two steps as observed for the reaction of **A1** with MeCCMe. Thus, coordination of $N_\beta Me_2$ to Ti forms **C9**, and then N_α−N_β cleavage proceeds through the TS **C9**−**10**. Because the $N_2^{SiH_3}N^{py}$ ligand is less compact (6-membered chelate rings) than $N_2^{SiH_3}N^{Me}$ and the metal center is less electrophilic, the intramolecular coordination of NMe_2 is less effective, and this results in an overall higher energy for both **C9** (6.4 kcal mol^{-1}) and the crucial transition state **C9**−**10** (25.5 kcal mol^{-1}) compared to **A9** (4.2 kcal mol^{-1}) and **A9**−**10** (22.0 kcal mol^{-1}).

Once **C10** is formed, NMe_2 transfer from Ti to C is easier than for **A10** ($\Delta G^\ddagger$ = 4.8 kcal mol^{-1} and ΔG = −3.1 kcal mol^{-1}), and the three isomers **C11**, **C12**, and **C13** have similar energies. The final step (TS **C13**−**6**, $\Delta G^\ddagger$ = 13.1 kcal mol^{-1}) is more difficult (relative to **C13**) than was the case for **A13**−**6**, but as **C13** is overall more stable than **A13**, the TS **C13**−**6** lies at a lower energy with respect to **C1** than does **A13**−**6** with respect to **A1**. Coordination of pyridine to **C6** (not shown in Scheme 7) affords the final insertion product. As in the mechanism starting from **A1**, the rate-determining step is the N_α−N_β bond cleavage step (**C9**−**10**).

Taking the Gibbs free energy of **A9**−**10** or **C9**−**10** with respect to separated reactants (**A1** or **C1** and MeCCMe) as an estimate of the activation energy, then the $\Delta\Delta G^\ddagger$ value of 3.5 kcal mol^{-1} between the two model systems translates into a ratio between the rate constants of between 2 and 3 orders of magnitude at room temperature, with the system **A** being the faster. Qualitatively, this is in good agreement with the relative rates of the real N_α−N_β insertion reactions **1** and **11** with PhCCMe (∼3 days and 5−10 min, respectively).

Conclusions

The closely related compounds Ti(N_2N^{py})($NNPh_2$)(py) (**1**) and Ti(N_2N^{Me})($NNPh_2$)(py) (**11**) have provided an excellent base for a detailed synthetic, mechanistic, and computational study of the reactions of titanium hydrazides with alkynes. Reactions of **1** with terminal and internal aryl alkynes ArCCR (Ar = Ph or substituted phenyl, R = Me or H) at room temperature give isolable Ti=N_α [2 + 2] cycloaddition products Ti(N_2N^{py}){N(NPh_2)C(R)CAr} with a specific regiochemistry (ArC bound to Ti). These are the first fully authenticated azametallacyclobutenes for any metal hydrazide. Electron-withdrawing aryl groups stabilize the metallacycles in the observed regiochemistry. Ti=N_α [2 + 2] cycloaddition products were also observed for **11** but were only stable below ∼−30 °C and with electron-deficient alkynes Ar^FCCMe (Ar^F= 4-$C_6H_4CF_3$ or C_6F_5).

Whereas reaction of **1** with PhCCMe at room temperature initially gives equilibrium mixtures of **1** and the cycloaddition product **2**, longer reaction times or gentle heating forms the vinyl imido product **10** in which PhCCMe has undergone net insertion into the N_α−N_β bond of **1**. The corresponding reactions of **11** with a range of alkynes RCCMe proceed smoothly at temperatures as low as −35 °C and follow pseudo-first-order kinetics with respect to **11**. DFT studies showed that the previously proposed mechanism[3] involving attack of the alkyne at N_β of an η^2-bound NNR_2 ligand is highly unfavorable due to the nucleophilic nature of N_β and the late nature of the C−N bond-forming transition state. Instead, a low-energy pathway involving initial alkyne cycloaddition to Ti=N_α followed by intramolecular coordination of NPh_2 precedes the actual N_α−N_β bond-breaking event. The calculated activation parameters for this process (modest $\Delta G^\ddagger_{298}$ and near-zero $\Delta S^\ddagger$) for realistic model systems were also fully consistent with experiment. The rate-limiting step in the N_α−N_β insertion process, nucleophilic attack of C_{Ti} at N_α (displacing NPh_2), is supported by a Hammett analysis of the rate constants and NPA charge analyses.

We reported in our preliminary communication[41] that **11** catalyzes (10 mol % loading) the 1,2-diamination of PhCCMe with Ph_2NNH_2 at room temperature *via* **13**, rather than undergoing the more widely established hydrohydrazination reaction. It is generally accepted that Group 4 hydrohydrazination catalysis proceeds *via* azatitanacyclobutenes.[50,61,62] The results presented here have shown that such metallacycles can also be intermediates en route to N_α−N_β insertion and hence can lead to alkyne diamination rather than hydrohydrazination. It was beyond the scope of this paper to develop these catalytic aspects; they will be the topic of future contributions from our laboratories. However, in terms of general future development of this reaction, the DFT calculations for Ti($N_2^{SiH_3}N^{Me}$)($NNMe_2$)(py) and Ti($N_2^{SiH_3}N^{Me}$)($NNPh_2$)(py) ($NNMe_2$ vs $NNPh_2$) show that insertion is not restricted only to hydrazides with phenyl substituents at N_β, thus pointing to the potential for considerable development of its scope and applications.

The supporting ligand also has a major role to play as it must allow $N_\beta R_2$ coordination along the reaction pathway but nonetheless stabilize terminal hydrazides in the first instance. Even for apparently similar ligands such as N_2N^{py} and N_2N^{Me} there can be several orders of magnitude difference in the reaction rate for the same alkyne. The electronic properties of the alkyne substrates are also critical. These govern the regiochemistry of the [2 + 2] cycloaddition intermediates which in turn define those in the arising N_α−N_β insertion products. Importantly, although electron-withdrawing aryl substituents in ArCCMe thermodynamically favor initial metallacycle formation (with ArC bound to Ti), electron-releasing Ar groups promote insertion (C_{Ti}−N_α bond formation). For reasons that are not yet clear (but which probably relate to the Brønsted acidity of sp C−H bonds), terminal alkynes do not undergo clean insertion reactions, although [2 + 2] cycloaddition products can be isolated in certain cases.

Our detailed mechanistic and theoretical studies of **1** and **11** explicitly connect M=N_α bond ("imide-like") and N_α−N_β bond reactivity along the same reaction coordinate. Given the rich chemistry of Group 4 metal−ligand multiple bonds in general,

it seems possible that all examples of $N_\alpha-N_\beta$ cleavage may proceed *via* initial addition to $Ti=N_\alpha$. As mentioned, Bergman has reported that reaction of *in situ* generated $Cp_2Zr(NNPh_2)$ with alkynes gave concomitant $N_\alpha-N_\beta$ cleavage (as opposed to insertion) and C−H activation reactions (Figure 1).[29] It is not apparent how (or whether) these products are related to those formed with **1** or **11**, but given the rich [2 + 2] cycloaddition chemistry of imido-zirconocenes with alkynes and other substrates in general,[49] it is likely that the complex sequence of steps leading from $Cp_2Zr(NNPh_2)$ involve azazirconacyclobutenes. This is consistent with Gade's very recent report of [2 + 3] cycloaddition products formed between $Zr(N_2{*}N^{py})(NNPh_2)(py)$ and organic azides.[55] In this system, an intermediate featuring a nitrene fragment (formed by N_2 loss from the first-formed [2 + 3] cycloaddition product) coupled across $Zr=N_\alpha$ is proposed to precede $N_\alpha-N_\beta$ cleavage, although no mechanistic studies or transition state calculations accompanied the experimental and DFT ground state results. Finally we note that the diazoalkane compound $Cp^*_2Ti\{\eta^2$-NNC(H)Tol} (homologues of which have been shown to have imido-like reactivity patterns[88,89]) undergoes $N_\alpha-N_\beta$ cleavage with CO to form a product with new $N_\alpha-CO$ and $Ti-N_\beta=C(H)Tol$ bonds[60] in a reaction reminiscent of that of $Cp_2Zr(NNPh_2)(DMAP)$ with CO forming $Cp_2Zr(NPh_2)(NCO)$ (Figure 1). It was postulated that attack of CO at the $M=N_\alpha$ bond of a terminal diazoalkane intermediate (without N_β coordination) precedes $N_\alpha-N_\beta$ cleavage. Our results are also consistent with this suggestion.

Experimental Section

Kinetic Measurements. A standard solution of *p*-methoxybenzene in toluene-d_8 was used for all kinetic experiments. The general procedure is as follows. In a glovebox, compound **11** (15.1 mg, 26.6 μmol) was weighed into a vial and dissolved in the standard solution (0.35 mL) and cooled to −45 °C. In a separate vial, RCCMe was dissolved in the standard solution (0.30 mL) and also cooled to −45 °C. The two vials were placed on a precooled tile and the solutions combined using a precooled pipet, agitated quickly, and transferred to a precooled J. Young NMR tube. The NMR tube was taken out of the glovebox and placed in a dry ice/isopropanol cold bath. The NMR probe was cooled to −35 °C and the sample added before being locked and shimmed. It was then warmed to −26 °C (other reaction temperatures were also used as appropriate as noted in the main text) and allowed to thermally equilibrate; the shimming was checked, and an array was set up recording a spectrum of 4 scans every 140 s. The ratios of the species were calculated by measuring the integrals of the trimethylsilyl groups relative to the internal standard. Pseudo-first-order rate contants were obtained from linear plots of $\ln([Ti]/[Ti]_0)$ vs time.

Computational Details. All calculations were performed with the Gaussian03 package[90] of programs with the hybrid B3PW91 functional.[91,92] The Ti atom was represented by the relativistic effective core potential (RECP) from the Stuttgart group and the associated basis set.[93] The remaining atoms (C, H, N, O, F) were represented by a 6-31G(d,p) basis set.[94] The Si atom was represented by RECP from the Stuttgart group and the associated basis set,[95] augmented by a d polarization function.[96] Full optimization of geometry was performed without any symmetry constraint, followed by analytical computation of the Hessian matrix to identify the nature of the located extrema as minima or transition states. Connection between reactant and product through a given transition state was checked by optimization of slightly altered geometries of the transition state along the two directions of the transition state vector associated to the imaginary frequency. All energies given in the text are Gibbs free energies ($T = 298$ K, $P = 1$ atm) in the gas phase

Acknowledgment. We thank the EPSRC for studentships to A.D. Schofield and J.D.S., a Ph.D plus postdoctoral award to J.D.S., and a postdoctoral fellowship to A.D. Schwarz. We also thank the Spanish MICINN for a MEC postdoctoral fellowship to A.N.

Supporting Information Available: General experimental methods and synthesis and characterization of the new compounds; details of the crystal structure determinations and full crystallographic data in CIF format for the structure determinations of **4**, **10**, **13**, **19**, **20**, and **24**; displacement ellipsoid plots of **19**, **20**, and **24**; preliminary structure determinations for **7** and **18**; variable temperature studies of the reaction of **11** with PhCCMe; optimized geometries for **A3**−**4**, **A12**, and **A13**; discussion of the influence of the hydrazide substituent ($NNMe_2$ vs $NNPh_2$) on the reaction mechanism and comparison of Gibbs free energy profiles for MeCCMe insertion into the $N_\alpha-N_\beta$ bond of **A1** and **B1**; complete reference 90 for Gaussian 03; DFT computed Cartesian coordinates for the optimized molecules and their electronic energies. This material is available free of charge *via* the Internet at http://pubs.acs.org.

JA1036513

(88) Polse, J. L.; Kaplan, A. W.; Andersen, R. A.; Bergman, R. G. *J. Am. Chem. Soc.* **1998**, *120*, 6316.
(89) Hanna, T. E.; Keresztes, I.; Lobkovsky, E.; Bernskoetter, W. H.; Chirik, P. J. *Organometallics* **2004**, *23*, 3448.
(90) Frisch, M. J.; et al. *Gaussian 03*, Revision D.01; Gaussian, Inc.: Wallingford, CT, 2004.
(91) Becke, A. D. *J. Chem. Phys.* **1993**, *98*, 5648.
(92) Perdew, J. P.; Wang, Y. *Phys. Rev. B* **1992**, *45*, 13244.
(93) Andrae, D.; Haussermann, U.; Dolg, M.; Stoll, H.; Preuss, H. *Theor. Chim. Acta* **1990**, *77*, 123.
(94) Hariharan, P. C.; Pople, J. A. *Theor. Chim. Acta* **1973**, *28*, 213.
(95) Bergner, A.; Dolg, M.; Kuchle, W.; Stoll, H.; Preuss, H. *Mol. Phys.* **1993**, *30*, 1431.
(96) Hollwarth, A.; Bohme, H.; Dapprich, S.; Ehlers, A. W.; Gobbi, A.; Jonas, V.; Kohler, K. F.; Stagmann, R.; Veldkamp, A.; Frenking, G. *Chem. Phys. Lett.* **1993**, *203*, 237.